Cell and fluid sampling microneedle patches for monitoring skin-resident immunity

Citation: Mandal, Anasuya et al. "Cell and fluid sampling microneedle patches for monitoring skin-resident immunity." Science Translational Medicine 10, 467 (November 2018): eaar2227 © 2018 The Authors

As Published: http://dx.doi.org/10.1126/scitranslmed.aar2227

Publisher: American Association for the Advancement of Science (AAAS)

Persistent URL: https://hdl.handle.net/1721.1/125769

Version: Author's final manuscript: final author's manuscript post peer review, without publisher's formatting or copy editing

Cell- and Fluid-Sampling Microneedle Patches for Monitoring Tissue-Resident Immunity

Authors: A. Mandal[1, 2] *, A. V. Boopathy[2], L.K.W. Lam[1,2], K.D. Moynihan[2,3], M.E. Welch[2], N. R. Bennett[2], M. E. Turvey[4], N. Thai[2], J. H. Van[3], J.C. Love[1,2,6,7], P. T. Hammond[1,2,4,6] & D. J. Irvine[2,3,5,6,7,8]

Affiliations:

[1]Department of Chemical Engineering, MIT, Cambridge, MA, USA.

[2]Koch Institute for Integrative Cancer Research, MIT Cambridge, MA, USA.

[3]Department of Biological Engineering, MIT, Cambridge, MA, USA.

[4]Infectious Diseases IRG, Singapore-MIT Alliance for Research and Technology, Singapore.

[5]Department of Materials Science and Engineering, MIT, Cambridge, MA, USA.

[6]Institute for Soldier Nanotechnologies, MIT, Cambridge, MA, USA.

[7]Ragon Institute of MGH, MIT, and Harvard, Cambridge, MA, USA.

[8]Howard Hughes Medical Institute, MD, USA.

One Sentence Summary: A minimally-invasive microneedle device allows repeated sampling of important tissue-resident immune cell populations from the skin.

Abstract:

Important immune cell populations reside within tissues and are not accessed by traditional blood draws used to monitor the immune system. To address this issue at an important barrier tissue, the skin, we created a microneedle (MN)-based technology for longitudinal sampling of cells and interstitial fluid, enabling minimally-invasive parallel monitoring of cellular and humoral immune responses in the skin. Solid MN projections were coated by a crosslinked biocompatible polymer, which swells upon skin insertion, forming a porous matrix for the infiltration of local leukocyte populations. By embedding molecular adjuvants and specific antigens encapsulated in nanocapsules within the hydrogel coating, antigen-specific lymphocytes can be enriched in the recovered cell population, allowing for subsequent detailed phenotypic and functional analysis. We demonstrate this approach in two animal models: mice immunized with a model protein antigen or infected in the skin with vaccinia virus. Following vaccination or infection, sampling MNs allowed tissue-resident memory T (T_{RM}) cells to be longitudinally monitored in the skin for

many months, during which time the antigen-specific T cell population in systemic circulation contracted to low or undetectable levels. Importantly, sampling MNs did not change the cellular or humoral immune status of naïve or antigen-exposed animals. This approach may be useful in vaccines and immunotherapies to temporally query T_{RM} populations, or as a diagnostic platform to sample for biomarkers in chronic inflammatory and autoimmune disorders, allowing information previously accessible only via invasive biopsies to be obtained in a minimally-invasive manner from the skin or other mucosal tissues.

[Main Text:]

Introduction

Current methods for accessing compartments of the body to obtain samples of tissues, cells, or fluid for medical diagnosis and monitoring fall into three categories: (i) invasive (in which a break in the skin is created, or where there is contact with mucosa or other internal body cavities beyond a natural or artificial body orifice, such as via traditional phlebotomy using venipuncture), (ii) minimally-invasive (involving minimal damage of tissues at the site of entry of instrument(s), such as saliva swabs obtained from the inner lining of the cheek) and, (iii) non-invasive (in which no skin-break or mucosal-contact occurs, such as urine collection). Immune monitoring is performed primarily by analysis of blood draws, a practice in use for millennia *(1)*, in which systemically circulating blood is drawn from a vein. In recent decades, immune monitoring by flow cytometry on peripherally-sampled blood has become the standard method for immunophenotyping *(2, 3)*. However, many important immune cell populations preferentially reside in peripheral tissues including barrier tissues such as the skin, gut, and other mucosal surfaces, and do not recirculate in the blood. This includes tissue-resident macrophages, natural killer cells, NK T cells, B cells, plasma cells, and memory T cells *(4–6)*. In particular, it is now understood that a larger proportion of T cells reside in peripheral tissues than in the secondary lymphoid organs at steady state *(7)*. Resident memory T cells (T_{RM}s) have been shown to permanently reside in the skin and other mucosal barrier tissues without recirculation in the blood *(8–10)*. T_{RM}s are cytotoxic $CD8^+$ T-cells poised for immediate interception and killing of infected cells upon re-exposure to their target antigen, which have recently been shown to provide a critical frontline response to diverse infections *(11)*. These cells are not accessed by traditional blood draw analysis of the immune response in humans.

Current minimally-invasive approaches for monitoring tissue-resident immune cell populations such as T_{RM}s are very limited. One widely used method to query the skin is via delayed type hypersensitivity tests *(12, 13)* such as the Mantoux test *(14)* and allergen patch tests *(15, 16)*, which offer qualitative readouts of an immune response towards a particular antigen. For example, in the case of the tuberculin Mantoux test, the tuberculin antigen is initially injected into the dermis and the skin is monitored for the next 2-3 days for the development of an induration, which indicates the presence of a recall immune response. It has been shown that the cells that respond to these injected stimuli are both central memory and effector memory cells, which traffic to the site of antigen deposition, as well as skin-resident antigen-specific T cells *(17)*. However, these methods remain qualitative and fail to offer quantitative information about the phenotypical and functional aspects of the cell infiltrate. There exist invasive methods of sampling and accessing non-recirculating immune cell populations from lymph nodes *(18)* or from skin *(19)* but these are apparatus-intensive and require special training for use. Minimally-invasive methods for

quantitative monitoring of the immune status of the skin or other barrier tissues could provide valuable information in the context of immunosuppression given to patients with genetic and acquired immunodeficiency disorders, organ transplants, and vaccination, but such methods are currently lacking.

MN patches, arrays of typically sub-mm pyramidal or conical projections designed to mechanically pierce the stratum corneum and reach the viable epidermis/upper dermis without engaging blood vessels following cutaneous application, have been extensively explored for delivery of drugs and vaccines into the skin *(20–24)*. However, a variety of MNs have also been designed to extract interstitial fluid (ISF) out of the skin, enabling monitoring of glucose, antibodies, or other biomarkers. Examples include the use of solid MNs to simply perforate the skin and enable access to ISF *(25, 26)*, hollow MNs that act as tiny syringes to collect ISF *(27, 28)*, MNs fabricated from hydrogels that swell on application to the skin to absorb ISF *(29, 30)*, microdialysis catheters *(31, 32)* or conjugation of proteins to the surface of solid MNs that capture specific analytes of interest during skin application *(33)*. While these are effective minimally-invasive technologies, to date only sampling of soluble biomolecules has been demonstrated.

Here we demonstrate a MN-based platform for the combined sampling of ISF and viable cells from the skin of mice, and demonstrate, for the first time, longitudinal monitoring of antigen-specific tissue-resident lymphocytes in the skin generated by vaccination or infection. Using solid MNs coated by a sampling hydrogel layer that swells on application to the skin, we demonstrate recovery of leukocytes that infiltrate the sampling layer. Mimicking the classical Mantoux test, we further show that by incorporation of antigen- and adjuvant-carrying nanoparticles into the sampling layer, forming Stimulatory Sampling Microneedles (SSMNs), we can specifically enrich for antigen-specific T_{RM}s and memory cells from the blood, without perturbing the immune status of the animals. Using a single-cell fluorescence based imaging technology, we characterize the phenotype of the sampling MN infiltrate to explore the mechanistic steps required in cell recruitment into the sampling MNs. Critically, SSMNs allow antigen-specific T_{RM}s to be traced in the skin at late times following vaccination or infection when circulating memory T cells are undetectable in the blood. This technology thus provides a novel means for minimally-invasive monitoring of key immune cell populations of interest in vaccination, infectious disease, and autoimmune disorders.

Results

Alginate-coated MNs for sampling cells and ISF

The conceptual design we pursued for a cell-sampling MN platform is outlined in **Fig. 1A**: A skin patch comprised of an array of 77 square pyramidal solid polymer MNs (each 250 μm in width at the base and ~600 μm in height) is coated with a biocompatible hydrogel layer that serves as a matrix for infiltrating cells. Embedded within the gel layer are adjuvants and lipid nanocapsules containing an antigen of interest (**Fig. 1A(a)**). Upon application to the skin, the hydrogel layer swells with the intake of ISF (**Fig. 1A(b)**), creating a biomaterial matrix supporting local cell infiltration into the coating. Antigen presenting cells (APCs) enter the alginate matrix in response to the localized inflammation induced by MN penetration into the skin *(34, 35)*, and are activated by the adjuvant present in the hydrogel layer to take up the embedded antigen-carrying nanocapsules (**Fig. 1A(c)**), allowing processing and presentation of the provided antigen. Cytokines and chemokines produced by these activated APCs in turn promote recruitment of T-

cells into the gel coating. T-cells specific for the antigen provided in the nanocapsules will be retained in the gel layer by prolonged interactions with the APCs *(36, 37)*, enriching these antigen-specific cells. Upon removal of the MNs from the skin, the hydrogel layer is dissolved to release recruited cells, which can then be analyzed by diverse immunological tools for phenotyping and immune profiling (**Fig. 1A(d-e)**). We hypothesized that such a design, if successful, would both allow factors in the ISF to be sampled and provide a window into the antigen-specific and non-specific immune cell populations that would be expected to respond in the skin, by mimicking early events following an actual infectious challenge.

To implement this design, polymer MN arrays were formed by melt-molding polylactide, as previously described *(38)*. Alginate was selected as the hydrogel coating material as this natural polysaccharide copolymer forms an ionically-crosslinked physical gel in the presence of non-toxic cations, and has proven to be biocompatible and safe in many biomedical applications *(39)*. Polylactide MNs were first coated with an absorbed layer of polylysine to promote electrostatic adhesion of the alginate to the underlying MN surface, followed by dropcasting of an alginate/sucrose solution, crosslinking of the alginate coating by application of a calcium chloride solution, and finally drying to a solid alginate/sucrose layer (**Fig. 1B**). Interbilayer-crosslinked multilamellar vesicles (ICMVs) *(40)*, ~125 nm diam. lipid nanocapsules carrying antigen and adjuvant (described further below), were incorporated into the alginate solution prior to dropcasting to incorporate these components into the alginate matrix and co-deliver these stimuli to infiltrating APCs. Sucrose was included in the gel coating layer to increase the mechanical integrity of the alginate coating during initial penetration of the stratum corneum and to act as an *in situ* porogen, increasing the porosity of the alginate when it is applied to the skin. Using Trypan blue to stain for sites of stratum corneum penetration post MN application, we confirmed that alginate/sucrose-coated MNs efficiently penetrated the skin of C57Bl/6 mice (**Fig. 1C**). MNs exposed to PBS for 20 minutes showed rapid rehydration and swelling of the alginate layer by ~3-fold in thickness from its dried state, as readily visualized by confocal microscopy (**Fig. 1D-F**).

We have previously shown that leukocytes can efficiently infiltrate alginate gels *in vivo (41)*. To optimize the alginate gel composition for cell recruitment, we compared cellular infiltration into subcutaneously implanted alginate gels composed of low or high molecular weight ("lo MW", 75,000 g/mol; and "hi MW", 200,000 g/mol) and with different alginate concentrations. We found that after 24 hr, basal cellular infiltration into alginate matrices was similar in Lo MW and Hi MW gels composed of 1 wt% alginate, which had an elastic modulus of ~1 KPa (**Fig. S1A-B**). Hi MW alginate was chosen because of better mechanical integrity and ease of handling.

Recovery of cells and ISF with sampling MNs

We were particularly interested in the question of whether MNs would sample antigen-specific skin T_{RM}s, and thus we first established a model immunization protocol in mice to generate a defined population of skin-resident T_{RM}. Groups of C57Bl/6 mice were primed and boosted subcutaneously with ovalbumin protein (OVA) and adjuvant. Four weeks later, blood and digested ear tissue were obtained from the animals or naïve control mice, stained with CFSE to distinguish cells from tissue digest debris, and OVA-specific $CD8^+$ T-cells expressing T_{RM} markers were identified by flow cytometry (**Fig. S2A**). We chose to define these cells conservatively as $CD69^+CD103^+$ T cells, although it is known that resident memory cells may lack expression of one or both of these markers in some tissues *(7)*. High levels of OVA-specific $CD8^+$

T-cells were detected in the blood of immunized mice at this time point (**Fig. S2B-C**). However, only the ear tissue from the immunized animals showed the presence of antigen-specific $CD69^+CD103^+$ T_{RMS} (**Fig. S2B-D**).

To evaluate the potential of alginate-coated MNs to sample tissue-resident cells and ISF, we first assessed their utility for recovering cells in a classic delayed type hypersensitivity/Mantoux test setting, in which an antigen is administered into the skin of immune animals to stimulate local antigen-specific lymphocyte accumulation (**Fig. 2A**). Groups of C57Bl/6 mice were immunized subcutaneously with ovalbumin protein (OVA) or left naïve as controls, and 4 weeks later, all animals were injected intradermally in the ear with the adjuvants polyI:C and pam3Cys mixed with 2 μg of OVA. Five days later, alginate-coated MNs containing no antigen or adjuvants in the gel coating were applied for 12 hours to the same skin site, and then retrieved for analysis. Processing of the cell sampling MNs was performed as outlined in **Fig. 2B**: the alginate layer was dissolved in the presence of EDTA, and recovered cells were stained with fluorochrome-labeled antibodies, labeled with CFSE to aid in distinguishing live cells from alginate debris, and analyzed by flow cytometry. In parallel, lymphocytes in peripheral blood were also analyzed for comparison. As shown in **Fig. 2C-D**, staining of lymphocytes from naïve mice with peptide-MHC tetramers revealed no OVA-specific $CD8^+$ T-cells in the blood, while OVA-specific T-cells were present at high levels in the circulation of immunized mice even at 4 weeks in response to the potent vaccination. Sampling MNs also recovered a large $tetramer^+$ population at the site of the antigen injection from immunized animals, though with lower total numbers of cells collected for analysis (**Fig. 2C-D**). In addition to cell recovery, the hydrogel layer of the MNs also samples ISF, which is difficult to access and is thus understudied. *In vitro*, MNs exposed to solutions of IgG or IgM and then digested for analysis of protein content by ELISA gave accurate measurements of the bulk solution concentration of IgG or IgM solutions (**Fig. S3**). We then compared OVA-specific IgG titers by ELISA on ISF recovered from the same MN patches vs. serum samples from the same animals. We were able to reliably quantify ova-specific IgG antibodies from MN recovered ISF (**Fig. 2E**). Consistent with prior measurements comparing serum and ISF *(42, 43)*, OVA-specific IgG was easily detected in MN-recovered ISF from immunized mice but showed a lower titer than serum from the same animals.

Adjuvant incorporation in the cell sampling layer increases cell recovery by sampling MNs

To simplify from the two-step Mantoux test-like sampling strategy as performed in the experiments of **Fig. 2**, we next investigated whether a one-time application of MNs loaded with adjuvant would suffice to recruit cells into the alginate matrix of the sampling patch. MN entry into the viable epidermis is expected to cause micro-tissue damage that provides a basal local inflammatory stimulus recruiting cells to the site *(34, 35)*. However, we hypothesized that inclusion of molecular adjuvants chosen for optimal stimulation of skin-derived APCs would further enhance cellular recruitment into the cell-sampling hydrogel layer of the MNs. Based on the expression of Toll-like receptors (TLRs) in keratinocytes and skin-derived dendritic cells, we explored the use of TLR3 agonist polyI:C (a potent double-stranded RNA adjuvant for stimulating anti-viral responses) as well as TLR1/2 agonist pam3Cys, a synthetic lipopeptide *(44–47)*. Intradermal injection of pam3Cys led to recruitment of CD8 T-cells and myeloid cells into the skin of C57Bl/6 mice, which was substantially augmented by co-administration of polyI:C (**Fig. S4A-B**). We next tested the functionality of these adjuvants when incorporated into an alginate gel. Inclusion of this adjuvant combination in alginate hydrogels implanted subcutaneously in the

flanks of eGFP mice (expressing GFP in all nucleated cells) also resulted in significantly higher cell infiltration into the gel after 24 hrs as quantified by confocal imaging of retrieved gels (**Fig. S4C-D**, the infiltration within Hi MW 1% gels without adjuvant can be seen in **Fig. S1B**).

PolyI:C is high molecular weight double-stranded RNA, which we expected to be retained effectively in the MN alginate coating, but pam3Cys is a small molecule lipopeptide. To promote retention of the latter and co-delivery of adjuvant signals with incorporated antigen to infiltrating APCs, we prepared ICMV lipid capsules loaded with pam3Cys. The ICMV capsules had a mean diameter of 126 ± 11 nm (**Fig. S5A**). We then assessed cellular recruitment into the gel layer of MNs carrying pam3Cys (either free or encapsulated in ICMVs) together with polyI:C in the alginate coating, which were applied to the skin of naïve mice for 24 hr. As shown in **Fig. S5B**, incorporation of pam3Cys and polyI:C into the alginate coating increased cellular infiltration into the MN, and incorporation of pam3Cys into ICMVs further enhanced cell recruitment ~8-fold over MNs carrying free pam3Cys.

We previously demonstrated that crosslinked ICMV lipid nanocapsules, which carried the antigen and pam3Cys adjuvant, have a high level of stability in physiological conditions, showing very low loss of encapsulated cargo over several days in the presence of serum*(40)*. As shown in **Fig. S6A**, there was no statistically significant drop in the quantity of polyI:C recovered from microneedles post 24 hr application to murine ear skin. In addition, polyI:C recovered from microneedles after 24 hr of patch application stimulated TLR3-expressing reporter cells in culture identically to polyI:C extracted from as-fabricated patches **(Fig. S6B)**. Thus, the polyI:C adjuvant is stable over the duration of sampling *in vivo*.

Inclusion of antigen in the sampling layer enhances recovery of antigen-specific lymphocytes by stimulatory sampling MNs

Incorporation of adjuvants in the gel layer should promote nonspecific recruitment of leukocytes in response to inflammatory cytokines/chemokines produced *in situ* by innate immune cells entering the alginate matrix, but such nonspecific cell sampling does not reflect the enrichment of antigen-specific lymphocytes that occurs rapidly at a site of infectious challenge *(48–51)*. In order to gain insight into local vaccine- or disease-specific immunological responses, we next introduced specific antigens into ICMVs carried in the cell sampling coating, co-encapsulating pam3Cys and the model antigen OVA to generate Stimulatory Sampling Microneedles (SSMNs). Dendritic cells can cross present protein antigen within a few hours of uptake *(52)*. As illustrated in **Fig. 1A**, our expectation was that APCs taking up antigen in the alginate matrix would present peptides *in situ* to recruited antigen-specific T cells, arresting their migration and egress from the alginate matrix in response to TCR signaling and thereby enriching for antigen-specific cells in the recruited T cell population.

To identify an effective sampling strategy that would not require pre-injection of antigen into the skin, we first investigated the effect of MN application time. SSMNs were prepared with alginate coatings carrying polyI:C and ICMVs co-loaded with pam3Cys and 2 μg OVA. SSMNs were applied for 12, 24 or 48 hours on the ears of C57Bl/6 mice that were previously immunized with OVA. These SSMN sampling groups were compared to animals that were sampled by a Mantoux-type experiment, where antigen and adjuvant were injected i.d. 60 hrs prior to application of MNs carrying no stimuli in the alginate coating (SMNs, **Fig. 3A**). Recovered cells were analyzed by flow cytometry to identify different infiltrating T-cell populations. As shown in **Fig.**

3B-C, 12 hr application of SSMNs to the skin of mice receiving no other pre-treatment recovered total live cells and $CD8^+$ T-cells in numbers comparable to alginate-only SMNs applied in the two-step "Mantoux" setting. Application of SSMNs for 24 hr increased the cell recovery another ~3-fold while sampling for 48 hrs increased cell recovery ~8 fold (**Fig. 3B-C**). On average, ~450 OVA-specific T cells were retrieved with 24 hr-applied SSMNs, ~9-10x more than SSMNs applied for 12 hrs, with only a minor further gain in OVA-specific cells for a 48 hr application time (**Fig. 3D-E**). Importantly, MNs applied for 24 hrs maximized the recovery of $CD3^+CD8^+CD69^+CD103^+$OVA-specific T_{RM} cells **(Fig. 3F-H)**. SSMNs applied to naïve mice showed no OVA-specific T-cell recovery (data not shown). Among OVA-specific T cells, we noted that a longer SSMN application time showed a trend towards recovery of more T cells recruited from the systemic circulation, and a corresponding lower proportion of OVA-specific T_{RM}s (**Fig. 3G**). Based on these findings we chose to focus on 24 hr SSMN sampling times, to maximize the recovered cell populations.

We next evaluated the impact of antigen inclusion in the cell-sampling layer on the composition of recovered leukocytes. As expected, antigen-loaded MNs were more effective in recovering antigen-specific T-cells, but also led to a generally higher recovery of total leukocytes (**Fig. 4A-E**). This may reflect rapid activation of antigen-specific T_{RM}s recruited to the MNs, which would both arrest these cells in the gel layer and trigger production by these cells of additional cytokines/chemokines that recruit additional leukocytes *(53, 54)*. As expected, OVA-specific $CD69^+CD103^+$ T_{RM} cells were not detected in the blood of these mice, but were recovered in substantial numbers using antigen-containing SSMNs (**Fig. 4E**).

To determine the threshold level of antigen that needed to be incorporated within the ICMVs to trigger an enrichment of antigen-specific cells in the SSMNs, we next titrated the dose of OVA incorporated in the MNs, with a fixed quantity of adjuvant in the MN coating during sampling (**Fig. 4F**). A notable increase in recovered antigen-specific and –non-specific T cells was observed when the MNs carried 2 μg of OVA compared to the lower doses of antigen (**Fig. 4G-J**). Approximately 5,000 live cells were typically recovered from a single MN array loaded with 2 μg antigen. Based on these studies, a 24 hour application with cell-sampling MNs incorporating 2 μg of antigen in ICMVs in the crosslinking layer of the alginate coating was designated as the optimized sampling strategy.

To gather more insight into events occurring during cell sampling, we further examined the cells recruited to SSMNs. Confocal microscopy performed on the gel layer of optimized SSMNs applied to the skin of OVA-immunized eGFP mice for 24 hours showed the presence of many cells infiltrating the alginate coating in close proximity to aggregates of ICMV particles (**Fig. 5A**). Scanning electron micrographs of recovered MNs also showed infiltrated lymphoid cells (diameter ~5-7 μm) embedded within the matrix displaying lamellar protrusions emanating in the cellular periphery (yellow arrows, **Fig. 5B**). These features were absent in control samples (**Fig. 5C**). In order to determine whether APCs infiltrating the MN coating interacted with ICMVs embedded within the alginate layer, we employed imaging cytometry, an image-based cytometry methodology ideal for analysis of sparse cell samples: Cells recovered by SSMNs were seeded in a nanowell array, stained with antibodies, and subsequently imaged in high throughput (**Fig. 5D**). Dual-labeled ICMVs encapsulating fluorescent OVA (AlexaFluor 555 conjugate) and the lipophilic tracer DiD were embedded in the alginate coating of SSMNs, and the MNs were applied for 24 hours on the ears of C57Bl/6 mice that had been immunized with OVA. Imaging cytometry analysis showed that 20% of recovered cells were T-cells ($CD3e^+$) and 15% were $CD19^+$ B cells (**Fig. 5E**). Approximately

20% of recovered cells were $CD45^+CD3e^-CD19^-CD11c^+$ APCs. Micrographs of individual nanowells containing the single cells showed live APCs containing bright fluorescent signal in the ICMV (DiD) channel and a weak OVA signal, suggesting uptake of OVA^-ICMVs by recruited dendritic cells in the gel layer (**Fig. 5F**). Essentially all $CD11C^+$ DCs recovered from the MNs were $ICMV^+$ (**Fig. 5G**). In addition, among $MHCII^+$ antigen presenting cells recovered from SSMNs, expression of the activation markers CD40 and CD86 were significantly increased compared to cells recovered from unstimulated naïve ear skin or cells sampled with MNs containing no antigen/adjuvants, in line with the expectation that the incorporated adjuvants activated recruited APCs **(Figs. 5H-I,** and **Fig. S7)**. Thus, relevant APCs efficiently acquired the antigen- and adjuvant-loaded nanocapsules and become activated on infiltration into the sampling MN matrix.

SSMNs do not immunize animals during sampling

As shown above, incorporation of specific antigen increases the local sampling of both antigen-specific cells and other leukocytes. However, a concern with this strategy is that recruited APCs might carry antigen from the MN matrix to draining lymph nodes, thereby immunizing the recipient and altering their immune status by the act of sampling. To test whether MN sampling immunizes animals, the skin of naïve C57BL/6 mice was sampled with SSMNs carrying OVA-ICMVs (**Fig. 6A**). As shown in **Fig. 6B** OVA-specific $CD8^+$ cells in the blood of these mice were undetectable before and after sampling, up to three weeks after MN application. As a positive control, the animals were subsequently vaccinated at 24 days post-sampling with 10 µg OVA in adjuvant, and 7 days later a clear $tetramer^+CD8^+$ T-cell population appeared in the blood. To further test whether SSMNs trigger any boosting to immune responses in the more sensitive setting of animals having pre-existing memory T-cells, the skin of C57BL/6 mice that had been immunized with OVA 36 weeks earlier was sampled with SSMNs. As shown in **Fig. 6C**, no significant difference was found in the frequency of antigen-specific $CD8^+$ cells in the blood of these mice before and after sampling, up to three weeks after MN application. Extending the SSMN application time to 48 hours also did not immunize the animals, as shown in **Fig. S8**, in both naïve and immunized mice.

Antibody responses can often be elicited by low doses of antigen reaching lymph nodes even under conditions where cross presentation of antigen to $CD8^+$ T-cells is negligible. We thus next assessed whether SSMNs induced changes in serum antibody titers against antigens carried in the MN gel matrix in the naïve or pre-immune settings. As shown in **Fig. 6D**, serum OVA-specific IgG titers also showed no change before and after sampling with MNs carrying 2 µg OVA in ICMVs, whether applied to naïve animals or animals previously immunized with OVA protein. Thus, sampling of cells/ISF from the skin by SSMNs does not appear to immunize or alter pre-existing T- or B-cell responses against target antigens.

Sampling MNs allow longitudinal monitoring of antigen specific resident-memory T cells

Having optimized the sampling MN platform and evaluated its baseline performance, we finally sought to demonstrate the capacity of this approach to follow T_{RM} populations in the skin of individual animals longitudinally. Continuing with the model antigen system, we primed and boosted groups of mice with OVA and adjuvant, then tracked skin-resident immune populations at 2-70 weeks after the booster immunization. Upon exposure to antigen, T cells first expand and then contract over time, and thus the proportion of SIINFEKL $tetramer^+$ (OVA-specific) $CD8^+$ T-cells in blood decreased

sharply in the 10 weeks following the boost, followed by a plateau stable population of circulating memory cells (**Fig. 7A-B**). In contrast, SSMNs revealed a tissue-resident population of antigen specific T-cells that decayed slightly over the same 10-week post boost period and then remained roughly constant for the next 60 weeks, reflecting their stable engraftment in the skin tissue. The population of T_{RM}s and OVA-specific T_{RM}s also remained unchanged when sampling via SSMNs, comparing 10 week and 36 week post boost time-points (**Fig. 7C-D**).

We next evaluated SSMNs for measuring TRMs following a live infectious challenge. C57Bl/6 mice were infected with vaccinia virus expressing SIVgag, via tail skin scarification *(55)*. SSMNs were prepared incorporating ICMV nanocapsules loaded with gag peptide, and cells were sampled from ear skin of the mice at 11 weeks post infection. We again found that the MN platform could detect longitudinally T_{RM}s and gag-specific T_{RM}s, which were not present in blood (**Fig. 7E-H**). The frequency of SIVgag-specific $CD8^+$ cells both in ear skin (sampled via MNs) and in systemic circulation (sampled via blood) was lower than in the OVA-immunized mouse model since the skin-scarification model is a weaker form of antigen-exposure compared to the OVA immunization. However, similar to the OVA immunization model, SSMNs detected a stable skin-resident antigen-specific T-cell population that was completely absent from the blood a few months post infection (**Fig. 7I-K**). Altogether, these results demonstrate the capacity of SSMNs to report longitudinally on skin-resident memory cell populations and provide quantitative information about antigen-specific T cells present in the tissues that are not detectable in the systemic circulation.

Proof of concept sampling of immune cells from human skin explants

We finally performed proof-of-concept studies to test whether SSMNs could perform similarly when applied to human skin. Sampling MNs with or without incorporated adjuvants were applied to fresh human skin obtained from abdominoplasty surgeries. Microneedles were applied *ex vivo* for 16 hours to skin samples maintained in a humid chamber at 37°C (**Fig. 8A**). Immunophenotyping via flow cytometry of sampled cells confirmed our findings in murine studies: MNs containing adjuvants sampled several thousand live cells per patch from human skin, and increased the number of $CD8^+$ and $CD11c^+$ cells recovered, compared to MNs without adjuvants (**Figs. 8B-D, S9**). These results establish the ability of SSMNs to minimally-invasively sample immune cell populations of interest, and further affirm the applicability of SSMNs for diagnostic sampling in human skin as well.

Discussion

Key roles for tissue-resident immune cells have been increasingly clarified over the last 10 years. T_{RM}s in particular have been revealed as critical players in long-lasting immunity, even in the absence of ongoing antigen presentation *(56)*, and provide front-line immune surveillance in the body's barrier tissues. T_{RM}s in both mice and humans have been implicated in immune protection in the lungs, skin, gut and other mucosal linings, enhancing immunity to both infections and tumors *(57)*. Investigation of T_{RM}s and their function in small animal models is usually achieved by sacrificing cohorts at defined time points to harvest their tissue, or by obtaining invasive biopsies from larger animals and humans, since T_{RM}s do not circulate in the blood and cannot be obtained from traditional blood draws.

Here, we present a microneedle-based, minimally invasive and painless system for monitoring tissue-resident humoral and cellular components of the immune system. This MN sampling platform enables isolation of live immune cells from the skin as well as ISF and biomarkers contained within it. By incorporating specific antigens within nanocapsules embedded within the cell-sampling alginate layer, SSMNs become a micro-Mantoux test and minimally-invasive biopsy in one, allowing target lymphocyte populations of interest to be enriched in the sampled population, mimicking the expected response to a genuine infectious challenge. Sampling MNs take the qualitative output of a classical delayed type hypersensitivity/Mantoux test and enable deep phenotypic and functional profiling of the responding antigen-specific tissue infiltrates. The ability to isolate live cells enables longitudinal analysis of functional traits of lymphocytes from the same animal/individual, traditional phenotyping, or advanced genomic methods such as single-cell RNA-seq. Optimized SSMNs enabled ~2,500 leukocytes to be recovered from a single 1 cm-diam. patch following a 24 hr application.

Key to the success of this approach was the identification of a MN design which could be infiltrated by cells but retained sufficient mechanical integrity to withstand the mechanical forces of skin insertion. With an ultimate goal of low cost, safe, disposable patches, we focused on MNs fabricated from melt-molded bioresorbable polymers. The MNs utilized in this work are applicable to human skin and are similar in design to the MNs used by other research groups for human use *(58–60)*. In preliminary studies we found that porous polymer MNs did not have sufficient mechanical integrity for skin insertion, consistent with the rapid decline in modulus of materials as volume percent porosity increases. By utilizing a dehydrated hydrogel coating over a solid "core" MN substrate, we were able to arrive at composition with a stable stiff surface layer during skin insertion, which could swell to provide a porous matrix amenable to cell infiltration *in situ*.

As shown in **Figs. 2C-D**, sampling MNs carrying no stimulus in the hydrogel layer could recover lymphocytes for analysis, likely attracted to the patch in response to cell death and cytokines/chemokines produced by keratinocytes and/or dendritic cells stimulated by the local physical micro-trauma of MN insertion *(61)*. However, we incorporated specific antigens and adjuvants into the sampling layer to both increase the number of recovered cells and to obtain a picture of the complete response expected if the skin were exposed to an infectious challenge-where both antigen and inflammatory cues would naturally be present. Incorporation of adjuvants into the gel layer increased cell recovery 2-fold over "empty" alginate coatings, and introduction of specific antigens further increased this recovery another ~4.5-fold in immunized animals. Notably, SSMNs containing both antigen and adjuvant recovered both more total live cells and more total antigen-specific T cells, reflecting that antigen presentation in the cell sampling layer led to production of cytokines/chemokines attracting both antigen-specific and -non-specific leukocytes.

Microneedles that release antigen and adjuvant into skin tissue are well known to effectively prime immune responses *in vivo (62–66)*. In response to inflammatory cues, Langerhans cells, dermal dendritic cells, and other APCs either resident or recruited to the skin will become activated, leading to upregulation of chemokine receptors that guide their migration to lymphatic vessels and draining lymph nodes, where captured antigen is presented to lymphocytes *(67, 68)*. We sought to circumvent this natural process during MN sampling by encapsulating our stimulatory antigen in nanocapsules physically entrapped within the alginate layer, to avoid dissemination of antigen into the surrounding tissue following MN application. SSMNs delivering small but non-negligible quantities of antigen/adjuvant did not lead to detectable priming of

antigen-specific T cells or antibody responses in treated mice, even if the animals had pre-existing memory populations against the sampling antigen. The fact that patch application for up to 48 hr did not stimulate an immune response suggests that APCs recruited to the microneedle coating are unable to migrate back out of the gel layer. We hypothesize that cells recruited into the alginate layer are shielded from chemokines produced by lymphatics that normally guide APCs to the draining lymph nodes, effectively trapping them in the microneedle coating. This will be an interesting aspect for further study in the future.

We believe that MN immune monitoring can impact at least three major areas of medicine: (1) enabling better disease management in autoimmune conditions by predicting oncoming disease flares, (2) monitoring tissue status in transplantation, as focused in our proof of concept work here, (3) monitoring vaccine responses. Methods for monitoring autoimmune diseases rely primarily on blood draws. However, cutaneous disorders such as lupus or psoriasis may be better served by biomarkers directly obtained from the skin. It is known that while ~ 83% of serum proteins are found in ISF, 50% of the proteins found in ISF are found in the interstitial fluid alone, and not in serum *(42)*. Monitoring for disease flares in lupus nephritis currently relies on the quantification of biomarkers such as anti-dsDNA, anti-nuclear antibodies, and anti-C1q from serum *(69, 70)*. Being able to potentially sample for these biomarkers from skin, in a painless and minimally-invasive manner, without the need of trained personnel for fluid withdrawal, could enable not only better compliance from patients for long-term monitoring purposes, but also more granular flare-prediction. Additionally, further characterization of the ISF could reveal novel biomarkers that are more predictive of the onset of flares, thereby enabling the ability to suppress or even avoid the onset of disease flares. In transplantation, recent work monitoring local reactions to skin transplants has suggested that donor T_{RM}s show early accumulations in allografts that will be rejected *(71)*. A minimally-invasive means to monitor for such reactions and pre-emptively provide immunosuppressive interventions could increase the lifetime of these grafts. And finally, as shown here in our preclinical models, tissue-resident memory T cell responses established by vaccination can be readily monitored with SSMNs.

A limitation with collecting cell and/or ISF samples using sampling MNs includes the size of the sample and possible limit-of-detection issues for methods that depend on high biomarker concentrations. On an average, ~ 5,000 live cells are obtained per MN array (1 cm^2) and about 1-2 μL of ISF. Of course, increasing the size of the MN array will linearly increase the sample size. Similar to the findings of other studies *(72)*, the area of sampling MN application healed within 2-3 days, with only minor erythema and inflammation for the first 24-48 hours.

In conclusion, this report demonstrates the applicability of sampling MNs for minimally-invasive longitudinal monitoring of the immune response, employing a painless sample collection method allowing the enumeration of tissue-specific cellular and secreted factors. We focused here on skin immune monitoring due to its importance for autoimmunity, transplants, and vaccines against bacterial and mosquito-borne pathogens, but MNs have been employed at many other mucosal sites such as buccal *(73)* and vaginal *(74)* surfaces, as well as applied to cutaneous tumors *(75, 76)*. We thus expect MN sampling to be relevant for many other applications beyond immune monitoring in the skin. This work holds promise to aid vaccine design and in the monitoring of long-term, chronic, auto-immune diseases.

Materials and Methods

Study Design

Rationale and design of study

The objective of this study was twofold: first, to sample resident-memory cell populations, not found in blood, from skin, via a minimally invasive skin patch, incorporating MNs and second, to assess the quantification of commonly found biomarkers in blood, e.g. antigen-specific IgG, as detected in interstitial fluid collected by MNs. All *in vivo* studies involving flow cytometric analysis were carried out in C57BL/6 mice in groups of four or more mice per treatment.

Mice

Animal studies were approved by the MIT IUCAC and animals were cared for in the USDA-inspected MIT Animal Facility under federal, state, local, and NIH guidelines for animal care. Female C57BL/6 mice 3-6 weeks of age and C57Bl/6 mice expressing GFP under control of the ubiquitin promoter were obtained from the Jackson Laboratory, and the colonies were maintained at the animal Koch Institute mouse facility at MIT.

Synthesis of ICMV lipid nanocapsules

Lipid nanocapsules were prepared as described previously with slight modifications *(40)*. All lipids were obtained from Avanti polar lipids and used without modification. Dried lipid films consisting of DOPC (1,2-dioleoyl-sn-glycero-3-phosphocholine) and MPB {1,2-dioleoyl-sn-glycero-3-phosphoethanolamine-N-[4-(pmaleimidophenyl)butyramide]} at a 1:1 molar ratio were rehydrated with cargo protein/peptide solutions (OVA protein, final concentration 0.1 mg/mL or AL11 peptide 0.1 mg/mL) and pam3Cys (Invivogen, final concentration 0.25 mg/mL) in 20mM bis-tris-propane in water (pH 7.0), followed by sonication and addition of dithiothreitol and $CaCl_2$ at final concentrations of 3 and 40 mM and incubation at 37°C for 1 hour, respectively, to induce fusion and cross-linking of lipid bilayers, followed by washing and PEGylation (MPEG-SH-2000, Laysan Bio) by adding 100 μL of 20 mg/mL PEG-thiol and incubating at 37°C for 30 minutes, followed by washing to obtain nanocapsules.

Atomic Force Microscopy measurements of alginate modulus

100 μL each of 1 wt % or 2 wt % solutions of SLM20 or SLG100 (Pronova) in PBS were mixed with 6.25μL of 5 wt% $CaCl_2$ in inserts of a 24-well Transwell plate. The mixture was immediately mixed via pipette after the addition of the $CaCl_2$ solution. The plate was then incubated for 15 minutes at 37°C, and 100 μL of PBS was added to each sample and allowed to swell for 24 hours at 37°C. The bottom membrane of the Transwell chambers was cut out and samples were pushed out onto glass slides with flat surface up. Elastic moduli of the wet gels was then measured using an MFP-3D-Bio (Asylum Research) AFM at the MIT Center for Materials Science and Engineering in force mode.

Fabrication of alginate-coated MNs

PDMS molds (Sylgard 184, Dow-Corning) for fabrication of MN arrays were prepared by laser micromachining *(77)*. Poly-L-lactide (Resomer® L 207 S, Evonik Industries AG) was melted over the molds under vacuum (−20 mm Hg, 200°C, 40 min). Poly-L-lysine (Sigma P4832, 0.01 wt%) solution was pipetted onto PLLA MNs for 30 mins, the solution was removed after 30 minutes, and the MNs were dried at 25°C. Alginate (Pronova SLG 100 or Pronova SLM 20, FMC Biopolymers) and sucrose (Sigma) solution (0.35 mg alginate, 1.4 mg sucrose in 60 μL of water) was pipetted onto each PLLA MN array and dried under vacuum at 25°C for at least 4 hours.

Crosslinking solution containing ICMV particles and poly I:C (Invivogen, HMW, average size 1.5kb – 8kb, 5 μg) and calcium (0.1 mg) in total volume of 50 μL was pipetted onto the surface of MNs and dried under vacuum for > 12 hours.

Subcutaneous gel injection studies

6-10 week old female C57BL/6 mice or UBI-GFP mice were co-injected with separate syringes containing 100 μL of alginate solution (SLG100 or SLM120), and 5 wt% calcium chloride solution in 20 μL water, under the dorsal flank. Animals were euthanized after 24 hours and gels were collected upon necropsy. Gels retrieved from UBI-GFP mice were imaged by confocal microscopy or analyzed via flow cytometry.

Immunizations

Lipid-conjugated CpG, a TLR9 agonist, was used as adjuvant for model protein immunizations. The sequence used was murine ODN class B sequence 1826 with two guanine spacers: 5'-*G*G*T*C*C*A*T*G*A*C*G*T*T*C*C*T*G*A*C*G*T*T-3' (*indicates phosphorothioate linkage). Solid phase DNA synthesis and 5' lipid conjugation were carried out as previously described using an ABI 394 synthesizer *(78)*. Following cleavage and deprotection, oligos were purified via RP-HPLC and quantified using UV-VIS. 6-10 week old female C57BL/6 mice were immunized via subcutaneous injection (at the tail base) with antigen (10 μg OVA, Worthington) along with 1.29 nmol lipo-CpG in 10 μL PBS. Control groups included naïve mice. Immune responses were characterized by flow cytometric analysis of antigen-specific T cell frequency (H-2K^b/SIINFEKL peptide-MHC tetramer staining), phenotypic marker expression, and ELISA analysis were carried to determine memory vs effector state of immune response.

Skin scarification

6-10 week old C57BL/6 mice were anesthetized using isolfluorane. Saline (5 μL) containing 2 x 10^6 PFU Vaccinia-SIVgag virus was applied to the tail skin 1 cm from the base of the tail. The skin area was then gently scratched 25 times with a 28 ½ G needle.

Skin application of MNs

Animals were anesthetized using isofluorane and ears of the mice were laid out flat on 3M Nexcare ™ waterproof tape. Alginate coated MNs, (with or without cargo of antigen and/or adjuvant in the gel coating), were applied by pressing down vertically with the thumb or index finger while securing Nexcare™ tape around the MN to keep it securely in place. Another layer of waterproof tape was secured around the first layer to keep the MN application site dry during the application period.

Processing of cells from gels and MNs, and Flow Cytometry

Subcutaneously injected gels were mashed using the backside of a syringe plunger and digested with alginate lyase (1mg/mL, Sigma A1603) and EDTA (0.02% of a stock solution pH 5.5) for 45 mins at 37°C with intermittent pipetting to break up the gel further. The solution was strained through at 50 μm cell strainer and pelleted. Frequencies of live cells were determined following staining with DAPI. Each alginate-coated MN retrieved from mouse ears was immersed in 200 μL of PBS containing 1% BSA and 100 mM EDTA and incubated at 37°C on a shaker at 150 rpm for 30 mins. The supernatant was collected and centrifuged to pellet cells. Recovered cells were resuspended in 100 μL of 0.36 μM CFSE in PBS for 5 minutes at 25°C for staining, quenched with 150 μL RPMI containing 10% FBS for 15 minutes and washed. Frequencies of antigen-specific

$CD8^+$ T-cells and their phenotypes were determined by flow cytometry analysis of the labeled cells following staining with anti-mouse antibodies (CD8α APC/Cy7, CD69 PE/Cy5, CD103 BV421) from Biolegend, and SIINFEKL/H-2Kb peptide–MHC tetramer (iTAg Tetramer/PE - H-2K$_b$ OVA (SIINFEKL), from MBL) or SIVgag tetramer (iTAg Tetramer/PE - H-2D$_b$ SIV GAG (AAVKNWMTQTL) from MBL), using a BD FACS Celesta HTS-1.

Multi-spectral Imaging Cytometry (MuSIC)

Cells were stained as described above with a cocktail of anti-mouse antibodies (CD8α PE/Cy7, CD19 BV711, MHCII PerCP710, CD11b BV655, CD11c PE/Cy5, CD3e PerCP, CD45 BV605, Sytox Green and CD103 BV421) from Biolegend. Stained cells were loaded onto a nanowell array, with loading governed by a rough Poisson distribution. The loaded nanowell arrays were then imaged with an epifluorescence microscope (Zeiss) with filter wheels at the relevant excitation and emission wavelengths. Compensation was performed with agarose beads (Agarose Beads Technologies) in 100 mM sodium carbonate. Each antibody was incubated with a separate aliquot of beads and imaged in all the fluorescent channels of interest. The percentage of spillover from other channels into a given channel was calculated from the fluorescence data and then used to compensate the acquired cell fluorescence data. Cells were identified from the obtained fluorescent images with Enumerator, an in-house image analysis software (Love Lab, MIT). For each nanowell array, a spreadsheet containing cell information including nanowell IDs, fluorescent intensities in each channel, and cell sizes, was generated. This data was then further analyzed and gated using Matchbox, an in-house MATLAB-based single-cell analysis software (Love Lab, MIT).

Human Skin Experiments

Ethics statement: Healthy human skin tissue was obtained from abdominoplastic surgery. The studies were approved by the respective institutional review boards (National Health Group Domain Specific Review Board (NHG DSRB 2012/00928) and Singhealth Centralized Institutional Review Board (CIRB 2011/327/E), respectively) and patients gave written informed consent. All skin samples were processed on the day of surgery.

MN patch application to explanted skin tissue: MNs were applied to explanted human skin samples, and adherence was maintained using a small petri-dish to provide downward pressure. These skin samples were maintained in a humid chamber for 16 hrs at 37°C, as shown in **Fig. 8A**.

Flow cytometry: CellTrace CFSE (Thermo C34554), CountBright absolute counting beads (Thermo C36950), CD3 APC (UCHT1, Biolegend), CD4 PE (RPA-T4, Biolegend), CD8 AF700 RPA-T8, Biolegend), CD45 V500 (HI30, BD Horizon), HLA-DR PECy7 (L243, BD Pharmingen), CD11c V450 (B-Ly6, BD Horizon), CD14 PerCPCy5.5 (HCD14, Biolegend).

Statistics

Data sets were analyzed using two-tailed nonparametric Mann-Whitney test, one or two-way analysis of variance tests, followed by Tukey's HSD test for multiple comparisons with Prism (GraphPad Software, San Diego, CA). p-values less than 0.05 were considered statistically significant. All values are reported as mean ± s.e.m.

Supplementary Materials:

Fig. S1: Optimization of alginate coating composition

Fig. S2: T_{RM} characterization in the blood and skin compartments in OVA-immunized mouse model.

Fig. S3. Analysis of fluids recovered from MNs accurately reports on surrounding solution concentrations.

Fig. S4: Cell recruitment is enhanced with the inclusion of adjuvants in the alginate hydrogel coating.

Fig. S5: ICMVs encapsulating antigen and adjuvant, when embedded in the alginate layer of sampling MNs, elicit increased recruitment of cells into sampling MNs.

Fig. S6: The activity of polyI:C is retained upon incorporation within sampling MNs.

Fig. S7: SSMNs containing adjuvants activate recruited APCs.

Fig. S8: SSMN application for up to 48 hours does not change the immune status of the animal.

Fig. S9: Gating strategy for cells obtained from sampling MNs applied to human skin.

References and Notes:

1. L. A. Parapia, History Of Bloodletting By Phlebotomy. *Br. J. Haematol.* **143**, 490–495 (2008).

2. M. Streitz, T. Miloud, M. Kapinsky, M. R. Reed, R. Magari, E. K. Geissler, J. A. Hutchinson, K. Vogt, S. Schlickeiser, A. H. Kverneland, C. Meisel, H.-D. Volk, B. Sawitzki, Standardization Of Whole Blood Immune Phenotype Monitoring For Clinical Trials: Panels And Methods From The One Study. *Transplant. Res.* **2**, 17 (2013).

3. V. Srinivasan, V. Pamula, M. Pollack, R. Fair, Clinical Diagnostics On Human Whole Blood, Plasma, Serum, Urine, Saliva, Sweat, And Tears On A Digital Microfluidic Platform, *Proc. MicroTAS*. 1287–1290 (2003).

4. E. Gomez Perdiguero, F. Geissmann, The Development And Maintenance Of Resident Macrophages. *Nat. Rev. Immunol.* **17**, 2–8 (2016).

5. Y. He, M. Shimoda, Y. Ono, I. B. Villalobos, A. Mitra, T. Konia, S. A. Grando, J. J. Zone, E. Maverakis, Persistence Of Autoreactive IgA-Secreting B Cells Despite Multiple Immunosuppressive Medications Including Rituximab. *JAMA Dermatology* **151**, 646–650 (2015).

6. D. K. Sojka, B. Plougastel-Douglas, L. Yang, M. A. Pak-Wittel, M. N. Artyomov, Y. Ivanova, C. Zhong, J. M. Chase, P. B. Rothman, J. Yu, J. K. Riley, J. Zhu, Z. Tian, W. M. Yokoyama, Tissue-Resident Natural Killer (NK) Cells Are Cell Lineages Distinct From Thymic And Conventional Splenic NK Cells. *Elife* **3**, E01659 (2014).

7. E. M. Steinert, J. M. Schenkel, K. A. Fraser, L. K. Beura, L. S. Manlove, B. Z. Igyártó, P. J. Southern, D. Masopust, Quantifying Memory CD8 T Cells Reveals Regionalization Of Immunosurveillance. *Cell* **161**, 737–749 (2015).

8. D. Masopust, V. Vezys, A. L. Marzo, L. Lefrançois, Preferential Localization Of Effector Memory Cells In Nonlymphoid Tissue. *Science* **291**, 2413–2417 (2001).

9. R. Purwar, J. Campbell, G. Murphy, W. G. Richards, R. A. Clark, T. S. Kupper, P. Proost, Ed. Resident Memory T Cells (T_{RM}) Are Abundant In Human Lung: Diversity, Function, And Antigen Specificity. *Plos One* **6**, E16245 (2011).

10. R. Watanabe, A. Gehad, C. Yang, L. L. Scott, J. E. Teague, C. Schlapbach, C. P. Elco, V. Huang, T. R. Matos, T. S. Kupper, R. A. Clark, Human Skin Is Protected By Four Functionally And Phenotypically Discrete Populations of Resident And Recirculating Memory T Cells. *Sci. Transl. Med.* **7**, 279ra39 (2015).

11. L. K. Beura, D. Masopust, Snapshot: Resident Memory T Cells. *Cell* **157**, 1488–1488.E1 (2014).

12. C. A. Black, Delayed Type Hypersensitivity: Current Theories With A Historic Perspective. *Dermatol. Online J.* **5**, 7 (1999).

13. A. R. Ahmed, Delayed-Type Hypersensitivity Skin Testing. *Arch. Dermatol.* **119**, 934–945 (1983).

14. M. Vukmanovic-Stejic, J. R. Reed, K. E. Lacy, M. H. A. Rustin, A. N. Akbar, Mantoux Test As A Model For A Secondary Immune Response In Humans. *Immunol. Lett.* **107**, 93–101 (2006).

15. J. M. Spergel, T. Brown-Whitehorn, The Use Of Patch Testing In The Diagnosis Of Food Allergy. *Curr. Allergy Asthma Rep.* **5**, 86–90 (2005).

16. R. Spiewak, Patch Testing For Contact Allergy And Allergic Contact Dermatitis. *Open Allergy J.* **1**, 42–51 (2008).

17. A. N. Akbar, J. R. Reed, K. E. Lacy, S. E. Jackson, M. Vukmanovic-Stejic, M. H. A. Rustin, Investigation Of The Cutaneous Response To Recall Antigen In Humans *In Vivo*. *Clin. Exp. Immunol.* **173**, 163–172 (2013).

18. D. Tatovic, P. Young, E. Kochba, Y. Levin, F. S. Wong, C. M. Dayan, Fine-Needle Aspiration Biopsy Of The Lymph Node: A Novel Tool For The Monitoring Of Immune Responses After Skin Antigen Delivery. *J. Immunol.* **195**, 386–392 (2015).

19. J. R. Bjerke, J. K. Livden, M. Degre, R. Matre, Interferon In Suction Blister Fluid From Psoriatic Lesions. *Br. J. Dermatol.* **108**, 295–299 (1983).

20. A. V. Romanyuk, V. N. Zvezdin, P. Samant, M. I. Grenader, M. Zemlyanova, M. R. Prausnitz, Collection Of Analytes From Microneedle Patches. *Anal. Chem.* **86**, 10520–10523 (2014).

21. S. R. Corrie, G. J. P. Fernando, M. L. Crichton, M. E. G. Brunck, C. D. Anderson, M. A. F. Kendall, Surface-Modified Microprojection Arrays For Intradermal Biomarker Capture, With Low Non-Specific Protein Binding. *Lab Chip* **10**, 2655–2658 (2010).

22. D. A. Muller, S. R. Corrie, J. Coffey, P. R. Young, M. A. Kendall, Surface Modified Microprojection Arrays For The Selective Extraction Of The Dengue Virus NS1 Protein As A Marker For Disease. *Anal. Chem.* **84**, 3262–3268 (2012).

23. K. T. Lee, D. A. Muller, J. W. Coffey, K. J. Robinson, J. S. Mccarthy, M. A. F. Kendall, S. R. Corrie, Capture Of The Circulating Plasmodium Falciparum Biomarker HRP2 In A Multiplexed Format. Via A Wearable Skin Patch, *Anal. Chem.* **86**, 10474–10483 (2014).

24. D. H. Keum, H. S. Jung, T. Wang, M. H. Shin, Y.-E. Kim, K. H. Kim, G.-O. Ahn, S. K. Hahn, Cancer Detection: Microneedle Biosensor For Real-Time Electrical Detection Of Nitric Oxide For In Situ Cancer Diagnosis During Endomicroscopy. *Adv. Healthc. Mater.* **4**, 1152–1152 (2015).

25. P. M. Wang, M. Cornwell, M. R. Prausnitz, Minimally Invasive Extraction Of Dermal Interstitial Fluid For Glucose Monitoring Using Microneedles. *Diabetes Technol. Ther.* **7**, 131–141 (2005).

26. Y. Ito, Y. Inagaki, S. Kobuchi, K. Takada, T. Sakaeda, Therapeutic Drug Monitoring Of Vancomycin In Dermal Interstitial Fluid Using Dissolving Microneedles. *Int. J. Med. Sci.* **13**, 271–276 (2016).

27. A. Jina, M. J. Tierney, J. A. Tamada, S. Mcgill, S. Desai, B. Chua, A. Chang, M. Christiansen, Design, Development, And Evaluation Of A Novel Microneedle Array-Based Continuous Glucose Monitor. *J. Diabetes Sci. Technol.* **8**, 483–487 (2014).

28. E. V. Mukerjee, S. D. Collins, R. R. Isseroff, R. L. Smith, Microneedle Array For Transdermal Biological Fluid Extraction And In Situ Analysis. *Sensors Actuators A Phys.* **114**, 267–275 (2004).

29. H. Chang, M. Zheng, X. Yu, A. Than, R. Z. Seeni, R. Kang, J. Tian, D. P. Khanh, L. Liu, P. Chen, C. Xu, A Swellable Microneedle Patch To Rapidly Extract Skin Interstitial Fluid For Timely Metabolic Analysis. *Adv. Mater.* (2017).

30. H. L. Quinn, M.-C. Kearney, A. J. Courtenay, M. T. C. Mccrudden, R. F. Donnelly, The Role Of Microneedles For Drug And Vaccine Delivery. *Expert Opin. Drug Deliv.* **11**, 1769–1780 (2014).

31. M. S. Angst, M. Tingle, M. Schmelz, B. Carvalho, D. C. Yeomans, Human In-Vivo Bioassay for the Tissue-Specific Measurement of Nociceptive and Inflammatory Mediators, *J. Vis. Exp.* (2008).

32. K. J. Hersini, L. Melgaard, P. Gazerani, L. J. Petersen, Microdialysis of Inflammatory Mediators in the Skin: A Review., *Acta Derm. Venereol.* **94**, 501–11 (2014).

33. J. W. Coffey, S. R. Corrie, M. A. F. Kendall, Early Circulating Biomarker Detection Using A Wearable Microprojection Array Skin Patch. *Biomaterials* **34**, 9572–9583 (2013).

34. S. M. Bal, J. Caussin, S. Pavel, J. A. Bouwstra, *In Vivo* Assessment Of Safety Of Microneedle Arrays In Human Skin. *Eur. J. Pharm. Sci.* **35**, 193–202 (2008).

35. A. C. I. Depelsenaire, S. C. Meliga, C. L. Mcneilly, F. E. Pearson, J. W. Coffey, O. L. Haigh, C. J. Flaim, I. H. Frazer, M. A. F. Kendall, Colocalization Of Cell Death With Antigen Deposition In Skin Enhances Vaccine Immunogenicity. *J. Invest. Dermatol.* **134**, 2361–2370 (2014).

36. S. P. Schoenberger, R. E. M. Toes, Ellen I H Van Der Voort, R. Offringa, C. J. M. Melief, T-Cell Help For Cytotoxic T Lymphocytes Is Mediated By CD40-CD40L Interactions. *Nature* **393**, 480–483 (1998).

37. E. Bell, T-cell Activation: T-cell-APC Interactions, *Nat. Rev. Immunol.* **4**, 930–930 (2004).

38. P. C. DeMuth, W. F. Garcia-Beltran, M. L. Ai-Ling, P. T. Hammond, D. J. Irvine, Composite Dissolving Microneedles for Coordinated Control of Antigen and Adjuvant Delivery Kinetics in Transcutaneous Vaccination, *Adv. Funct. Mater.* **23**, 161–172 (2013).

39. J. Hong, N. J. Shah, A. C. Drake, P. C. DeMuth, J. B. Lee, J. Chen, P. T. Hammond, Graphene Multilayers as Gates for Multi-week Sequential Release of Proteins from Surfaces, *ACS Nano* **6**, 81–8 (2012).

40. J. J. Moon, H. Suh, A. Bershteyn, M. T. Stephan, H. Liu, B. Huang, M. Sohail, S. Luo, S. H. Um, H. Khant, J. T. Goodwin, J. Ramos, W. Chiu, D. J. Irvine, Interbilayer-crosslinked Multilamellar Vesicles as Synthetic Vaccines for Potent Humoral and Cellular Immune Responses, *Nat. Mater.* **10**, 243–51 (2011).

41. Y. Hori, P. J. Stern, R. O. Hynes, D. J. Irvine, Engulfing Tumors with Synthetic Extracellular Matrices for Cancer Immunotherapy, *Biomaterials* **30**, 6757–67 (2009).

42. J. Kool, L. Reubsaet, F. Wesseldijk, R. T. Maravilha, M. W. Pinkse, C. S. D'Santos, J. J. Van Hilten, F. J. Zijlstra, A. J. R. Heck, Suction Blister Fluid as Potential Body Fluid for Biomarker Proteins, *Proteomics* **7**, 3638–3650 (2007).

43. M. P. Hedger, S. Herriarachchi, Measurement of Immunoglobulin G Levels in Adult Rat Testicular Interstitial Fluid and Serum, *J. Androl.* **15**, 583–590 (1994).

44. W. C. Weldon, V. G. Zarnitsyn, E. S. Esser, M. T. Taherbhai, D. G. Koutsonanos, E. V. Vassilieva, I. Skountzou, M. R. Prausnitz, R. W. Compans, M. M. Rodrigues, Ed. Effect of Adjuvants on Responses to Skin Immunization by Microneedles Coated with Influenza Subunit Vaccine, *PLoS One* **7**, e41501 (2012).

45. Y. Lai, A. Di Nardo, T. Nakatsuji, A. Leichtle, Y. Yang, A. L. Cogen, Z.-R. Wu, L. V Hooper, R. R. Schmidt, S. von Aulock, K. A. Radek, C.-M. Huang, A. F. Ryan, R. L. Gallo, Commensal Bacteria Regulate Toll-like Receptor 3–dependent Inflammation After Skin Injury, *Nat. Med.* **15**, 1377–1382 (2009).

46. B. S. Baker, J.-M. Ovigne, A. V. Powles, S. Corcoran, L. Fry, Normal keratinocytes express Toll-like Receptors (TLRs) 1, 2 and 5: Modulation of TLR Expression in Chronic Plaque Psoriasis, *Br. J. Dermatol.* **148**, 670–679 (2003).

47. V. Flacher, M. Bouschbacher, E. Verronèse, C. Massacrier, V. Sisirak, O. Berthier-Vergnes, B. de Saint-Vis, C. Caux, C. Dezutter-Dambuyant, S. Lebecque, J. Valladeau, Human Langerhans Cells Express A Specific TLR Profile and Differentially Respond to Viruses and Gram-positive Bacteria, *J. Immunol.* **177** (2006) (available at http://www.jimmunol.org/content/177/11/7959).

48. W. Weninger, M. Biro, R. Jain, Leukocyte Migration in the Interstitial Space of Non-lymphoid Organs, *Nat. Rev. Immunol.* **14**, 232–46 (2014).

49. T. Gebhardt, L. M. Wakim, L. Eidsmo, P. C. Reading, W. R. Heath, F. R. Carbone, Memory T cells in Nonlymphoid Tissue that Provide Enhanced Local Immunity During Infection with Herpes Simplex Virus, *Nat. Immunol.* **10**, 524–30 (2009).

50. R. L. Modlin, C. Pirmez, F. M. Hofman, V. Torigian, K. Uyemura, T. H. Rea, B. R. Bloom, M. B. Brenner,

Lymphocytes Bearing Antigen-specific γδ T-cell Receptors Accumulate in Human Infectious Disease Lesions, *Nature* **339**, 544–548 (1989).

51. J. A. Wiley, R. J. Hogan, D. L. Woodland, A. G. Harmsen, Antigen-specific CD8(+) T cells Persist in the Upper Respiratory Tract Following Influenza Virus Infection, *J Immunol* **167**, 3293–3299 (2001).

52. P. Guermonprez, L. Saveanu, M. Kleijmeer, J. Davoust, P. van Endert, S. Amigorena, ER–phagosome Fusion Defines an MHC Class I Cross-presentation Compartment in Dendritic Cells, *Nature* **425**, 397–402 (2003).

53. J. M. Schenkel, K. A. Fraser, V. Vezys, D. Masopust, Sensing and Alarm Function of Resident Memory CD8(+) T cells, *Nat Immunol* **14**, 509–513 (2013).

54. J. M. Schenkel, K. A. Fraser, L. K. Beura, K. E. Pauken, D. Masopust, V. Vezys, D. Masopust, Resident Memory CD8 T Cells Trigger Protective Innate and Adaptive Immune Responses, *Science (80-.).* **346**, 98–101 (2015).

55. L. Liu, R. C. Fuhlbrigge, K. Karibian, T. Tian, T. S. Kupper, Dynamic Programing of CD8+ T cell Trafficking After Live Viral Immunization, *Immunity* **25**, 511–520 (2006).

56. L. K. Mackay, A. T. Stock, J. Z. Ma, C. M. Jones, S. J. Kent, S. N. Mueller, W. R. Heath, F. R. Carbone, T. Gebhardt, Long-lived Epithelial Immunity by Tissue-resident memory T (T_{RM}) Cells in the Absence of Persisting Local Antigen Presentation, *Proc. Natl. Acad. Sci.* **109** (2012).

57. S. N. Mueller, L. K. Mackay, Tissue-resident Memory T Cells: Local Specialists in Immune Defence, *Nat. Rev. Immunol.* **16**, 1–11 (2015).

58. H. S. Gill, D. D. Denson, B. A. Burris, M. R. Prausnitz, Effect of Microneedle Design on Pain in Human Volunteers., *Clin. J. Pain* **24**, 585–94 (2008).

59. P. González-Vázquez, E. Larrañeta, M. T. C. McCrudden, C. Jarrahian, A. Rein-Weston, M. Quintanar-Solares, D. Zehrung, H. McCarthy, A. J. Courtenay, R. F. Donnelly, Transdermal Delivery of Gentamicin Using Dissolving Microneedle Arrays for Potential Treatment of Neonatal Sepsis, *J. Control. Release* **265**, 30–40 (2017).

60. H. L. Quinn, C. M. Hughes, R. F. Donnelly, *In Vivo* and Qualitative Studies Investigating the Translational Potential of Microneedles for Use in the Older Population., *Drug Deliv. Transl. Res.* **8**, 307–316 (2018).

61. A. Takeuchi, Y. Nomoto, M. Watanabe, S. Kimura, Y. Morimoto, H. Ueda, Application of Microneedles to Skin Induces Activation of Epidermal Langerhans Cells and Dermal Dendritic Dells in Mice, *Biol. Pharm. Bull.* **39**, 1309–1318 (2016).

62. S. P. Sullivan, D. G. Koutsonanos, M. Del Pilar Martin, J. W. Lee, V. Zarnitsyn, S.-O. Choi, N. Murthy, R. W. Compans, I. Skountzou, M. R. Prausnitz, Dissolving Polymer Microneedle Patches for Influenza Vaccination., *Nat. Med.* **16**, 915–20 (2010).

63. M. Zaric, O. Lyubomska, O. Touzelet, C. Poux, S. Al-Zahrani, F. Fay, L. Wallace, D. Terhorst, B. Malissen, S. Henri, U. F. Power, C. J. Scott, R. F. Donnelly, A. Kissenpfennig, Skin Dendritic Cell Targeting *via* Microneedle Arrays Laden with Antigen-Encapsulated Poly- d , l -lactide- *co* -Glycolide Nanoparticles Induces Efficient Antitumor and Antiviral Immune Responses, *ACS Nano* **7**, 2042–2055 (2013).

64. M. Zaric, O. Lyubomska, C. Poux, M. L. Hanna, M. T. McCrudden, B. Malissen, R. J. Ingram, U. F. Power, C. J. Scott, R. F. Donnelly, A. Kissenpfennig, Dissolving Microneedle Delivery of Nanoparticle-Encapsulated Antigen Elicits Efficient Cross-Priming and Th1 Immune Responses by Murine Langerhans Cells, *J. Invest. Dermatol.* **135**, 425–434 (2015).

65. K. Matsuo, S. Hirobe, Y. Yokota, Y. Ayabe, M. Seto, Y.-S. Quan, F. Kamiyama, T. Tougan, T. Horii, Y. Mukai, N. Okada, S. Nakagawa, Transcutaneous Immunization Using A Dissolving Microneedle Array Protects Against Tetanus, Diphtheria, Malaria, and Influenza., *J. Control. Release* **160**, 495–501 (2012).

66. P. C. Demuth, Y. Min, B. Huang, A. D. Miller, J. A. Kramer, D. H. Barouch, P. T. Hammond, D. J. Irvine, Polymer Multilayer Tattooing for Enhanced DNA Vaccination, *Nat. Mater.* **12**, 367–376 (2013).

67. A. Mildner, S. Jung, Development and Function of Dendritic Dell Subsets, *Immunity* **40**, 642–656 (2014).

68. T. Worbs, S. I. Hammerschmidt, R. Förster, Dendritic Cell Migration in Health and Disease, (2016),

doi:10.1038/nri.2016.116.

69. A. Matrat, C. Veysseyre-Balter, P. Trolliet, E. Villar, F. Dijoud, J. Bienvenu, N. Fabien, Simultaneous Detection of Anti-C1q and Anti-double Stranded DNA Autoantibodies in Lupus Nephritis: Predictive Value for Renal Flares., *Lupus* **20**, 28–34 (2011).

70. J. M. Ahearn, C.-C. Liu, A. H. Kao, S. Manzi, Biomarkers for Systemic Lupus Erythematosus., *Transl. Res.* **159**, 326–42 (2012).

71. C. G. Lian, E. M. Bueno, S. R. Granter, A. C. Laga, A. P. Saavedra, W. M. Lin, J. S. Susa, Q. Zhan, A. K. Chandraker, S. G. Tullius, B. Pomahac, G. F. Murphy, Biomarker Evaluation of Face Transplant Rejection: Association of Donor T cells with Target Cell Injury, *Mod. Pathol.* **27**, 788–99 (2014).

72. K. Mooney, J. C. McElnay, R. F. Donnelly, Children's Views on Microneedle Use as an Alternative to Blood Sampling for Patient Monitoring, *Int. J. Pharm. Pract.* **22**, 335–344 (2014).

73. Y. Ma, W. Tao, S. J. Krebs, W. F. Sutton, N. L. Haigwood, H. S. Gill, Vaccine Delivery to the Oral Cavity Using Coated Microneedles Induces Systemic and Mucosal Immunity, *Pharm. Res.* **31**, 2393–2403 (2014).

74. N. Wang, Y. Zhen, Y. Jin, X. Wang, N. Li, S. Jiang, T. Wang, Combining Different Types of Multifunctional Liposomes Loaded with Ammonium Bicarbonate to Fabricate Microneedle Arrays as a Vaginal Mucosal Vaccine Adjuvant-dual Delivery System (VADDS), *J. Control. Release* **246**, 12–29 (2017).

75. C. Wang, Y. Ye, G. M. Hochu, H. Sadeghifar, Z. Gu, Enhanced Cancer Immunotherapy by Microneedle Patch-assisted Delivery of Anti-PD1 Antibody, *Nano Lett.* **16**, 2334–2340 (2016).

76. Q. Zeng, J. M. Gammon, L. H. Tostanoski, Y.-C. Chiu, C. M. Jewell, *In Vivo* Expansion of Melanoma-specific T Cells Using Microneedle Arrays Coated with Immune-polyelectrolyte Multilayers, *ACS Biomater. Sci. Eng.* **3**, 195–205 (2017).

77. P. C. Demuth, J. J. Moon, H. Suh, P. T. Hammond, D. J. Irvine, Releasable Layer-by-layer Assembly of Stabilized Lipid Nanocapsules on Microneedles for Enhanced Transcutaneous Vaccine Delivery, *ACS Nano* **6**, 8041–8051 (2012).

78. H. Liu, K. D. Moynihan, Y. Zheng, G. L. Szeto, A. V Li, B. Huang, D. S. Van Egeren, C. Park, D. J. Irvine, Structure-based Programming of Lymph-node Targeting in Molecular Vaccines, *Nature* **507**, 519–22 (2014).

Acknowledgments: The authors would like to thank K. Rakhra, T. Tokatlian, E. L. Dane, T. Gierahn, M. B. Melo and H. Watkins for their technical expertise and help in making this work possible. **Funding:** This work was supported in part by the Ragon Institute of MGH, MIT, and Harvard, the Koch Institute Support (core) Grant P30-CA14051 from the National Cancer Institute and the U. S. Army Research Laboratory and the U. S. Army Research Office through the Institute for Soldier Nanotechnologies, under contract number W911NF-13-D-0001. D.J.I. is an investigator of the Howard Hughes Medical Institute. **Author Contributions:** A.M., A.V.B., P.T.H., and D.J.I. designed the experiments, analyzed the data, and carried out statistical analyses. A.M. and A.V.B. carried out material characterization. A.M synthesized the SSMNs and carried out *in vivo* experiments. A.M., D.J.I., P.T.H., and J.C.L. wrote the manuscript. L.K.W. designed and performed imaging cytometry experiments. K.D.M. prepared material for OVA and lipo-CpG vaccinations. M.E.W. designed and performed the AFM experiments. N.R.B. provided technical support for fluorophore labeling of alginate. N.R.B and N.T. performed protein quantification accuracy and polyI:C stability experiments. M.E.T. performed the human skin sampling MN experiments. J.H.V. provided technical support for SSMN preparation and *in vivo* studies. **Competing Interests:** The authors declare no competing interests.

Figures:

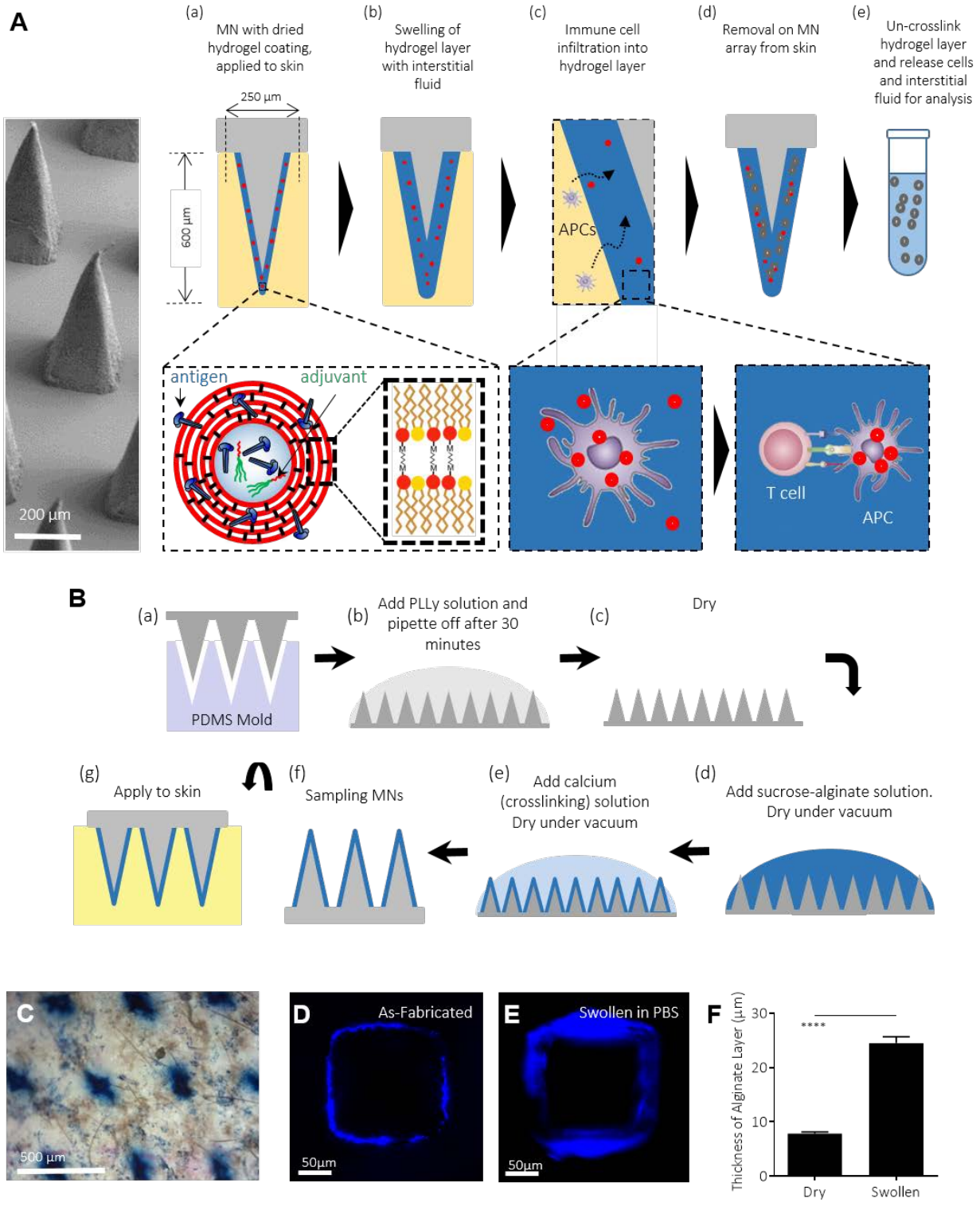

Figure 1: Fabrication of Stimulatory Sampling Microneedles (SSMNs) platform for immune monitoring. (A) Schematic of SSMN structure and proposed mechanisms of action for cell and interstitial fluid sampling. **(B)** Microneedle fabrication process: (a) Arrays were fabricated by melt-

molding poly-L-Lactide into PDMS molds; (b) Poly-L-lysine (PLL) was absorbed to arrays from solution for 30 minutes, rinsed and (c) dried; (d) Sucrose-alginate solution was deposited onto PLL-coated arrays and dried under vacuum; (e) Calcium solution was added to the alginate/sucrose layer and dried under vacuum; (f) The resulting sampling MNs were stored under vacuum before (g) application to skin. **(C)** Trypan blue stain of mouse ear tissue showing effective penetration of MNs. Scale bar 500 µm. (D-F) Confocal micrographs showing a cross section of the alginate layer (blue) on an individual MN projection before **(D)** and after **(E)** swelling in PBS for 20 minutes at 25°C (scale bar 50 µm). **(F)** Thickness of alginate layer quantified before/after PBS swelling.

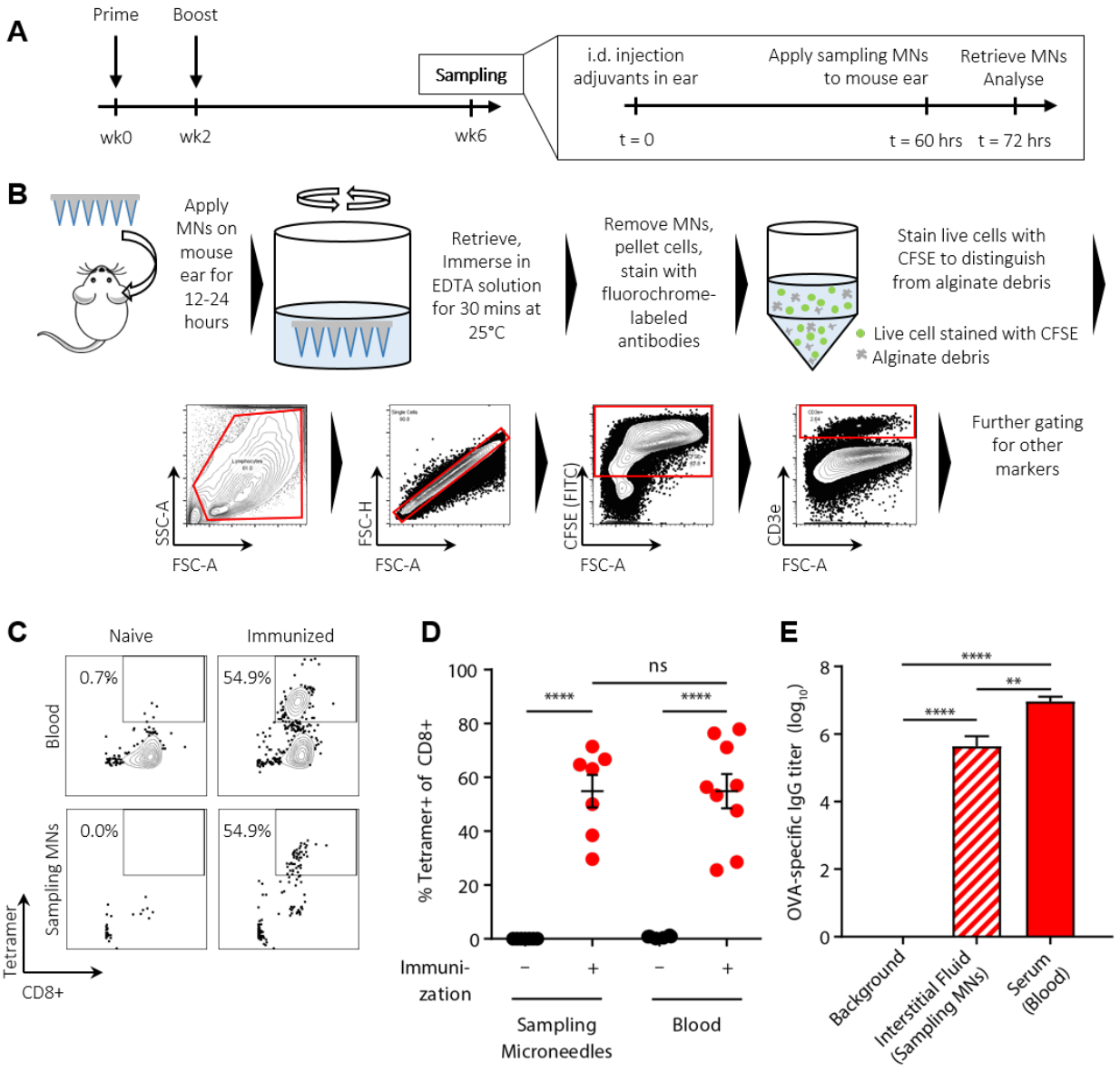

Figure 2: Cell sampling MNs allow tandem analysis of cellular and humoral immune responses. (A) Groups of OVA-immunized or naïve C57Bl/6 mice (*n*=9/group) were injected intradermally in the ear at time zero with 2 µg OVA and 5 µg each of polyI:C and Pam3Cys. Sixty

hr later, sampling MN were applied to the same site for 12 hr, followed by retrieval for flow cytometry analysis. **(B)** Workflow of sample processing and flow cytometry gating strategy. **(C)** Representative flow cytometry plots showing OVA-specific $CD8^+$ cells in naïve and immunized mice, as sampled from blood or with cell-sampling MNs, identified by labeling with SIINFEKL/H-$2K^b$-streptavidin tetramers. **(D)** OVA-specific cells as a percentage of total $CD8^+$ cells quantified via flow cytometry. **(E)** OVA-specific IgG titer (log_{10}) as quantified from serum (from blood) and interstitial fluid (from sampling MNs). Data shown are means ± s.e.m. from one representative of two independent experiments. ns, nonsignificant, **, $p < 0.01$, ****, $p < 0.0001$, analyzed by one-way ANOVA, followed by Tukey's HSD.

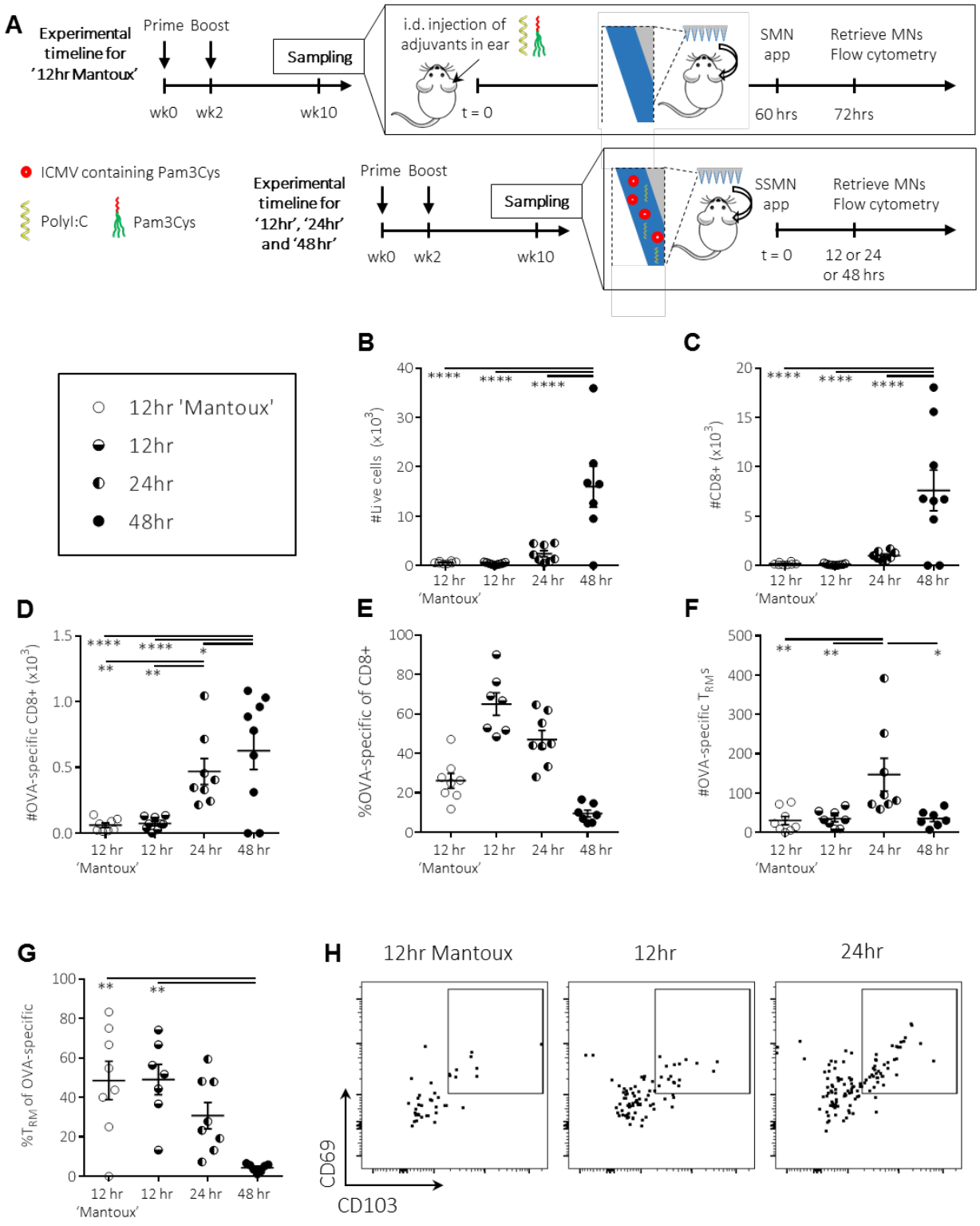

Figure 3: Microneedles incorporating adjuvants enable single-step sampling of antigen-specific T_{RM}s. (A) Timeline and schematic of sampling time optimization experiment in OVA-immunized C57Bl/6 mice (*n*=5/group). **(B-H):** Enumeration of recovered total live cells **(B)**, CD8+ cells **(C)**, OVA-specific CD8+ cells **(D)**, frequency of OVA-specific cells among CD8+ cells **(E),**

OVA-specific TRMs **(F)**, frequency of TRMs among OVA-specific cells **(G)**, and representative flow cytometry analysis of TRM markers CD69 and CD103 on CD8+ cells **(H)**. Cell counts are per MN patch. Data shown are mean ± s.e.m. from one representative of three independent experiments. *, p<0.05, **, p<0.01, and ****, p < 0.0001 analyzed by one-way ANOVA, followed by Tukey's HSD.

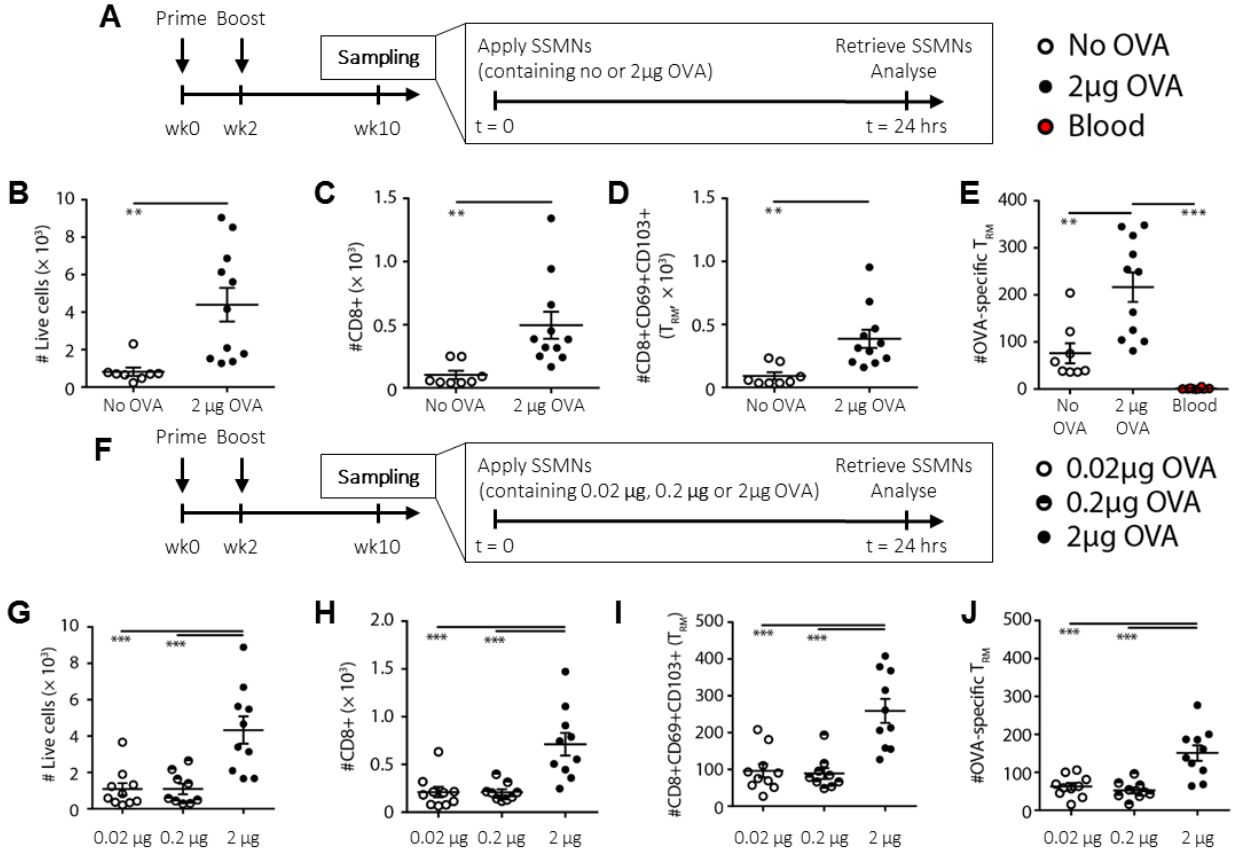

Figure 4: SSMNs containing antigen-loaded nanocapsules enrich sampling for antigen-specific T_{RM}s. (A-E) Groups of OVA-immunized C57Bl/6 mice (*n*=6/group) were sampled with MNs applied to the ear according to the timeline **(A)**. Enumeration of recovered total live cells **(B)**, $CD8^+$ cells **(C)**, $CD8^+CD69^+CD103^+$ T_{RM}s **(D)** and OVA-specific T_{RM}s **(E)**, per SSMN array, from SSMNs containing empty ICMV nanocapsules or ICMVs loaded with 2ug OVA. **(F-J)** Groups of OVA-immunized C57Bl/6 mice (*n*=5/group) were sampled with MNs applied to the ear according to the timeline **(F)**. Enumeration of recovered total live cells **(G)**, $CD8^+$ cells **(H)**, $CD8^+CD69^+CD103^+$ T_{RM}s **(I)** and OVA-specific T_{RM}s **(J)**, per SSMN array, from SSMNs containing ICMVs encapsulating 0.02µg, 0.2µg or 2µg OVA. Data shown are mean ± s.e.m. from one representative of two to three independent experiments. **, p<0.01, *** and p < 0.001 analyzed by one-way ANOVA, followed by Tukey's HSD.

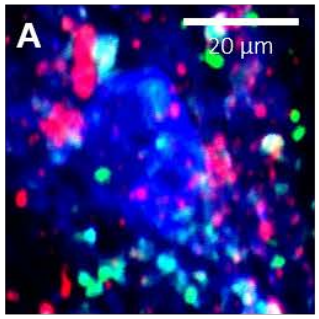
A
20 µm

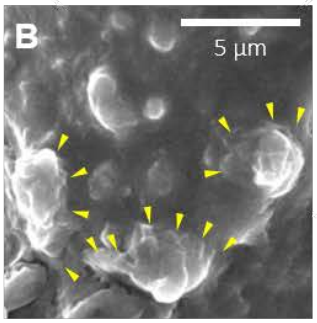
B
5 µm

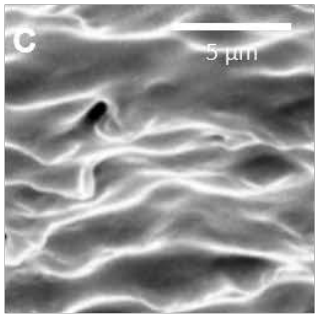
C
5 µm

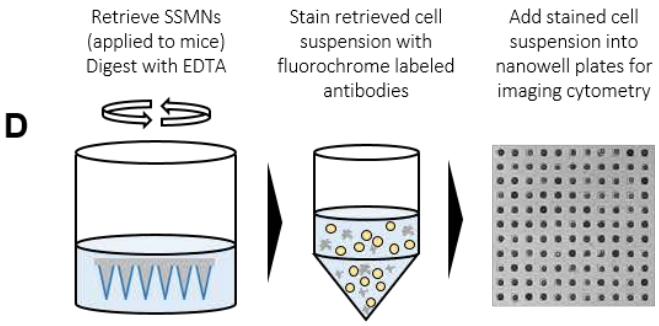
D
Retrieve SSMNs (applied to mice) Digest with EDTA
Stain retrieved cell suspension with fluorochrome labeled antibodies
Add stained cell suspension into nanowell plates for imaging cytometry

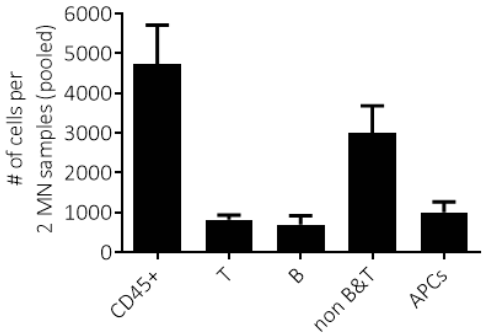
E
# of cells per 2 MN samples (pooled)
6000
5000
4000
3000
2000
1000
0
CD45+
T
B
non B&T
APCs

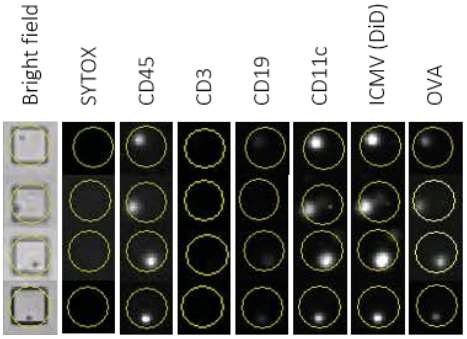
F
Bright field
SYTOX
CD45
CD3
CD19
CD11c
ICMV (DiD)
OVA

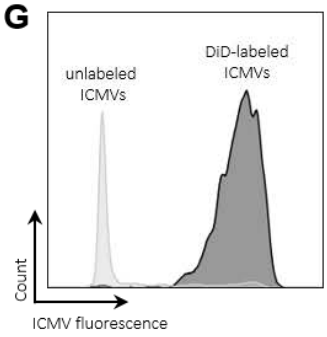
G
unlabeled ICMVs
DiD-labeled ICMVs
Count
ICMV fluorescence

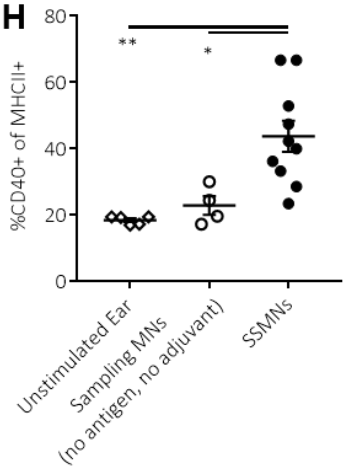
H
%CD40+ of MHCII+
80
60
40
20
0
**
*
Unstimulated Ear
Sampling MNs (no antigen, no adjuvant)
SSMNs

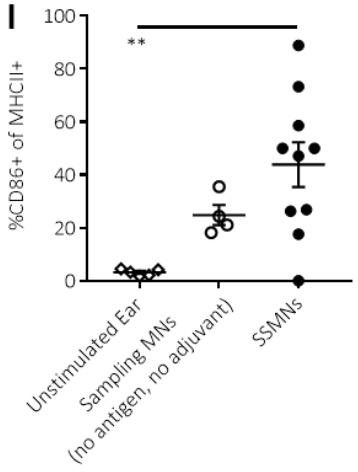
I
%CD86+ of MHCII+
100
80
60
40
20
0
**
Unstimulated Ear
Sampling MNs (no antigen, no adjuvant)
SSMNs

Figure 5: Sampling MNs containing ICMV nanocapsules accumulate antigen-loaded dendritic cells. (A) Confocal micrograph showing the surface of SSMNs coated with alginate (blue) containing embedded ICMVs (red) and recruited cells (green) following application to the skin of eGFP transgenic mice. Scale bar 20 μm. **(B)** Scanning electron micrographs of SSMNs post-application to mouse ear skin for 24 hours showing lymphocytes, approximately 5μm in diameter, with bright lamellar features (indicated with white arrows), that are not observed in the pre-applied SSMN platform **(C)**. **(D-G)** SSMNs containing 5 μg of polyI:C and DiD-labeled ICMVs encapsulating 2 μg Alexa Fluor555-labeled OVA and 5 μg pam3Cys were applied to the ears of OVA-immunized mice (*n*=3/group) for 24 hours, followed by retrieval, antibody staining and phenotypic analysis via imaging cytometry. **(D)** Schematic of imaging cytometry. **(E)** Cell phenotypes obtained from SSMNs. **(F)** Representative imaging cytometry raw data showing overlay of fluorescent channels for live/dead dye Sytox, CD45, CD3, CD19, CD11c, DiD (ICMV) and OVA-Alexa Fluor 555, showing the presence of antigen presenting cells containing ICMVs. The edges of each well are 50 μm. **(G)** Representative 2D imaging cytometry plots gated on showing OVA/ICMV fluorescence in CD45+CD11c+ dendritic cells for labeled vs. control ICMVs. **(H-I)** SSMNs applied to naïve mouse ears sampled a higher proportion of activated $MHCII^+$ antigen presenting cells compared to MNs without antigens or adjuvants, and unstimulated naïve ear tissue. Data shown are mean ± s.e.m. from one representative of two to three independent experiments. *, $p<0.05$, **, and $p<0.01$ analyzed by one-way ANOVA, followed by Tukey's HSD.

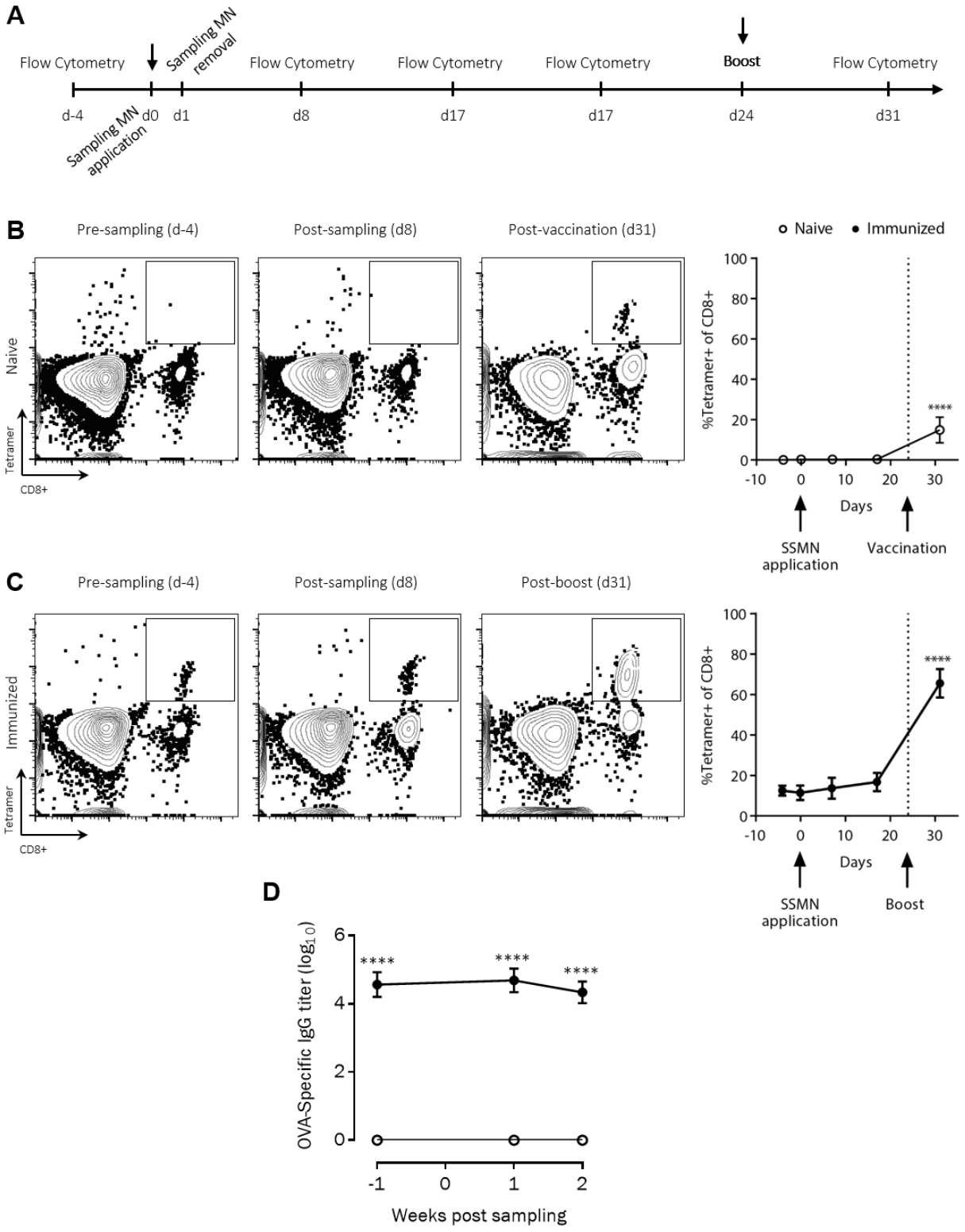

Figure 6: Sampling MNs do not change the immune status of the animal. SSMNs containing adjuvants and ICMVs loaded with 2 μg of OVA were applied to the ear skin of naïve or OVA-immunized C57Bl/6 mice (*n*=5/group) for 24 hours, then retrieved and analyzed via flow

cytometry. Shown are experimental timeline **(A)** representative flow cytometry plots and quantification of OVA-specific CD8+ T cells from blood in naïve **(B)** and previously immunized **(C)** mice, before and after SSMN application at day 0 and vaccination on day 24. **(D)** Serum OVA-specific IgG titers pre- and post-sampling with SSMNs. Data shown are mean ± s.e.m. from one representative of two independent experiments. ****: $p < 0.0001$ analyzed by one-way ANOVA, followed by Tukey's HSD.

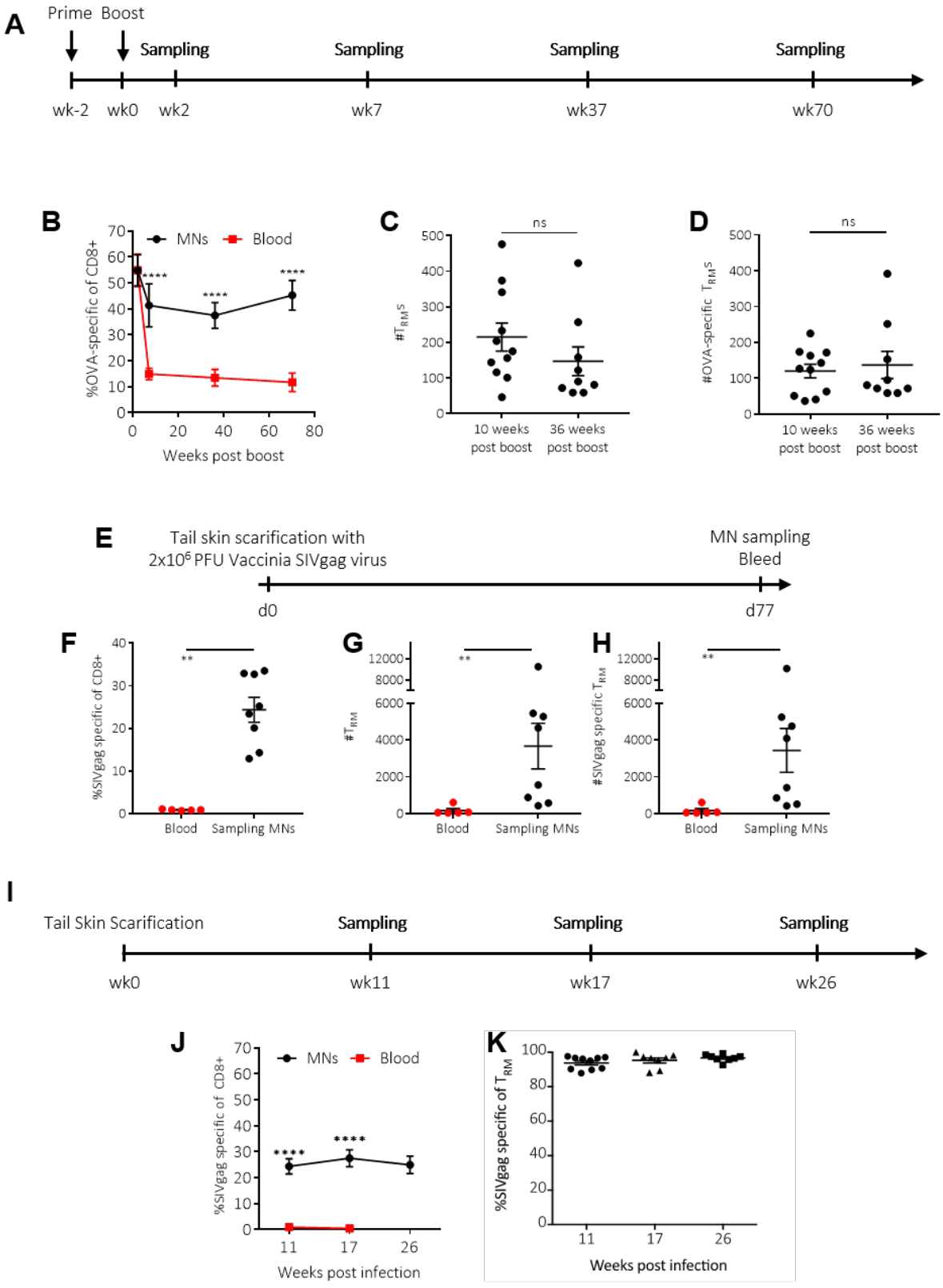

Figure 7: Sampling MNs reveal a stable population of TRMs in skin up to a year post vaccination or infection. (A-D) Groups of C57Bl/6 mice (*n*=5/group) were primed and boosted

with OVA and adjuvant, and then repeatedly sampled using SSMNs and blood draws over 70 weeks post boost to trace antigen-specific T cells in the skin and peripheral blood. **(A)** Timeline of experiment. **(B)** Flow cytometry analysis of OVA-specific $CD8^+$ T cells (C), T_{RM}s, and OVA-specific T_{RM}s (D), quantified from SSMNs and blood. **(E-H)** Groups of C57Bl/6 mice (*n*=5/group) were infected with $2x10^6$ PFU of SIVgag-expressing vaccinia virus via tail skin scarification and sampled beginning 11 weeks post infection via blood draws or SSMNs applied to the ear containing ICMVs (2 μg AL11 SIVgag peptide and 5 μg pam3Cys) and 5 μg polyI:C. After 24 hours, patches were retrieved and analyzed via flow cytometry. Experimental timeline **(E)**, frequency of SIVgag $tetramer^+CD8^+$ cells **(F)**, enumeration of $CD8^+CD69^+CD103^+$ T_{RM} cells **(G)** and SIVgag-specific T_{RM}s **(H)** from blood and SSMNs. **(I-K)** Timeline **(I)**, frequency of SIVgag-specific $CD8^+$ T cells **(J)** and frequency of SIVgag-specific T_{RM}s **(K)**, quantified from SSMNs and blood, when sampled at various times post vaccinia infection. Data shown are mean ± s.e.m. from one representative of two to three independent experiments, analyzed by Wilcox-Mann-Whitney test **(F-H)**, one-way ANOVA **(K)** or two-way ANOVA **(B, J)**, ns, nonsignificant, **p < 0.01, ***p < 0.001, ****, p < 0.0001.

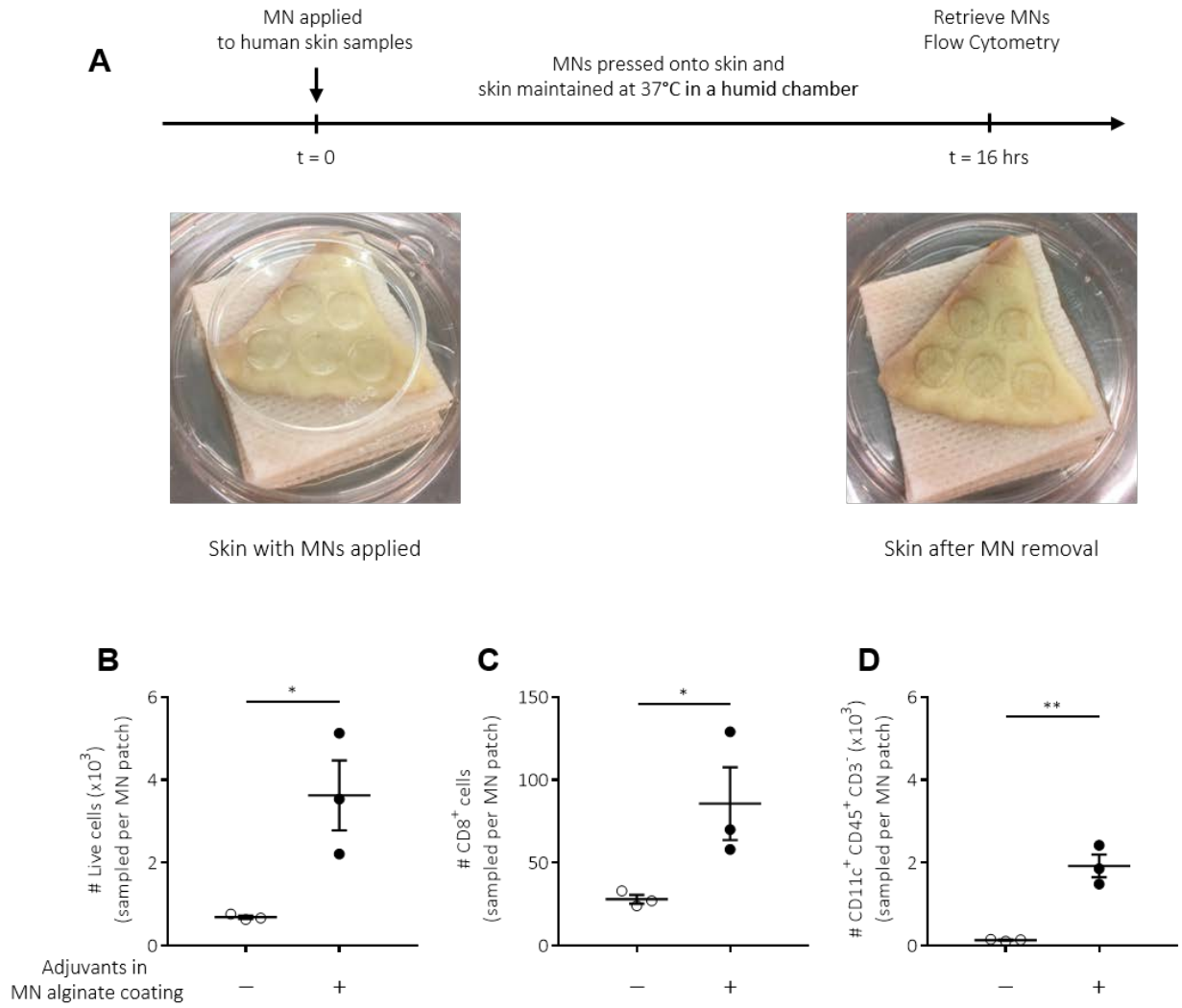

Figure 8: SSMNs enable sampling of lymphocytes from human skin. SSMNs were applied to excised human skin for 16 hrs, and then gel coatings were digested for analysis of recovered cells via flow cytometry. **(A)** Timeline and photographs of the experimental setup. **(B-D)** Enumeration of recovered total live cells **(B)**, $CD8^+$ cells **(C)**, $CD11c^+CD45^+$ cells **(D)**, per sampling MN array, from MNs containing no adjuvants, or SSMNs containing polyI:C and ICMVs encapsulating pam3Cys. Data shown are mean ± s.e.m., analyzed by two-tailed nonparametric Mann-Whitney test, *$p < 0.05$, **$p < 0.01$.

Supplementary Materials:

Supplementary Material for

Cell- and Fluid-Sampling Microneedle Patches for Monitoring Tissue-Resident Immunity

A. Mandal, A. V. Boopathy, L.K.W. Lam, K.D. Moynihan, M.E. Welch, N. R. Bennett, M. E. Turvey, N. Thai, J. H. Van, J.C. Love, P. T. Hammond & D. J. Irvine*

*Corresponding author. E-mail: djirvine@mit.edu

This file includes:

Fig. S1: Optimization of alginate coating composition.

Fig. S2: T_{RM} characterization in the blood and skin compartments in OVA-immunized mouse model.

Fig. S3. Analysis of fluids recovered from MNs accurately reports on surrounding solution concentrations.

Fig. S4: Cell recruitment is enhanced with the inclusion of adjuvants in the alginate hydrogel coating.

Fig. S5: ICMVs encapsulating antigen and adjuvant, when embedded in the alginate layer of sampling MNs, elicit increased recruitment of cells into sampling MNs.

Fig. S6: The activity of polyI:C is retained upon incorporation within sampling MNs.

Fig. S7: SSMNs containing adjuvants activate recruited APCs.

Fig. S8: SSMN application for up to 48 hours does not change the immune status of the animal.

Fig. S9: Gating strategy for cells obtained from sampling MNs applied to human skin.

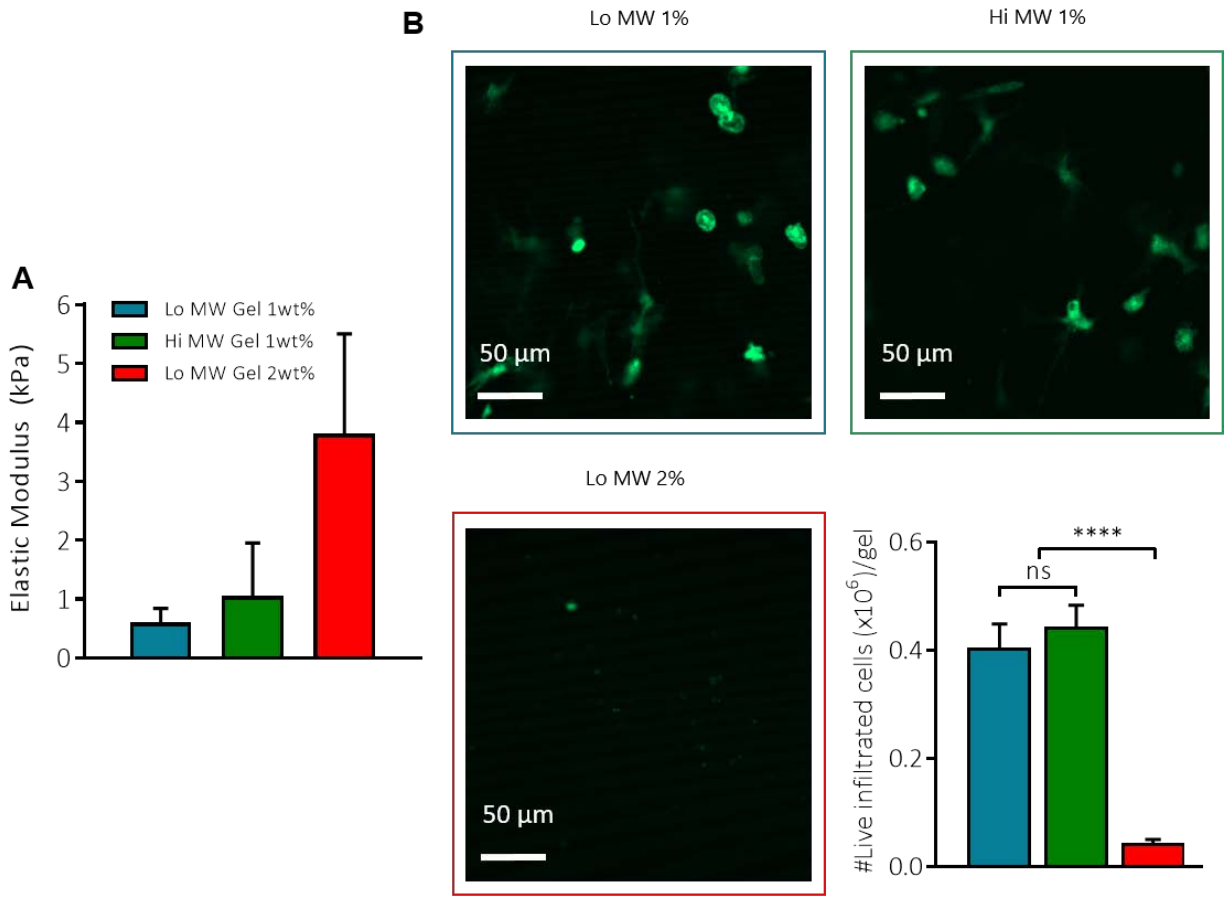

Figure S1: Optimization of alginate coating composition. (A) Elastic modulus as measured by atomic force microscopy of low (75,000 g/mol) and high (200,000 g/mol) molecular weight gels, at 1% and 2% w/w of gel. **(B)** Basal infiltration of cells into alginate gels when subcutaneously injected for 24 hours under the dorsal flank skin of EFGP-transgenic mice, as visualized by confocal microscopy and infiltrated live cell counts using a hemocytometer. Data shown are mean ± s.e.m., analyzed by one-way ANOVA, ns, nonsignificant, ****, $p < 0.0001$.

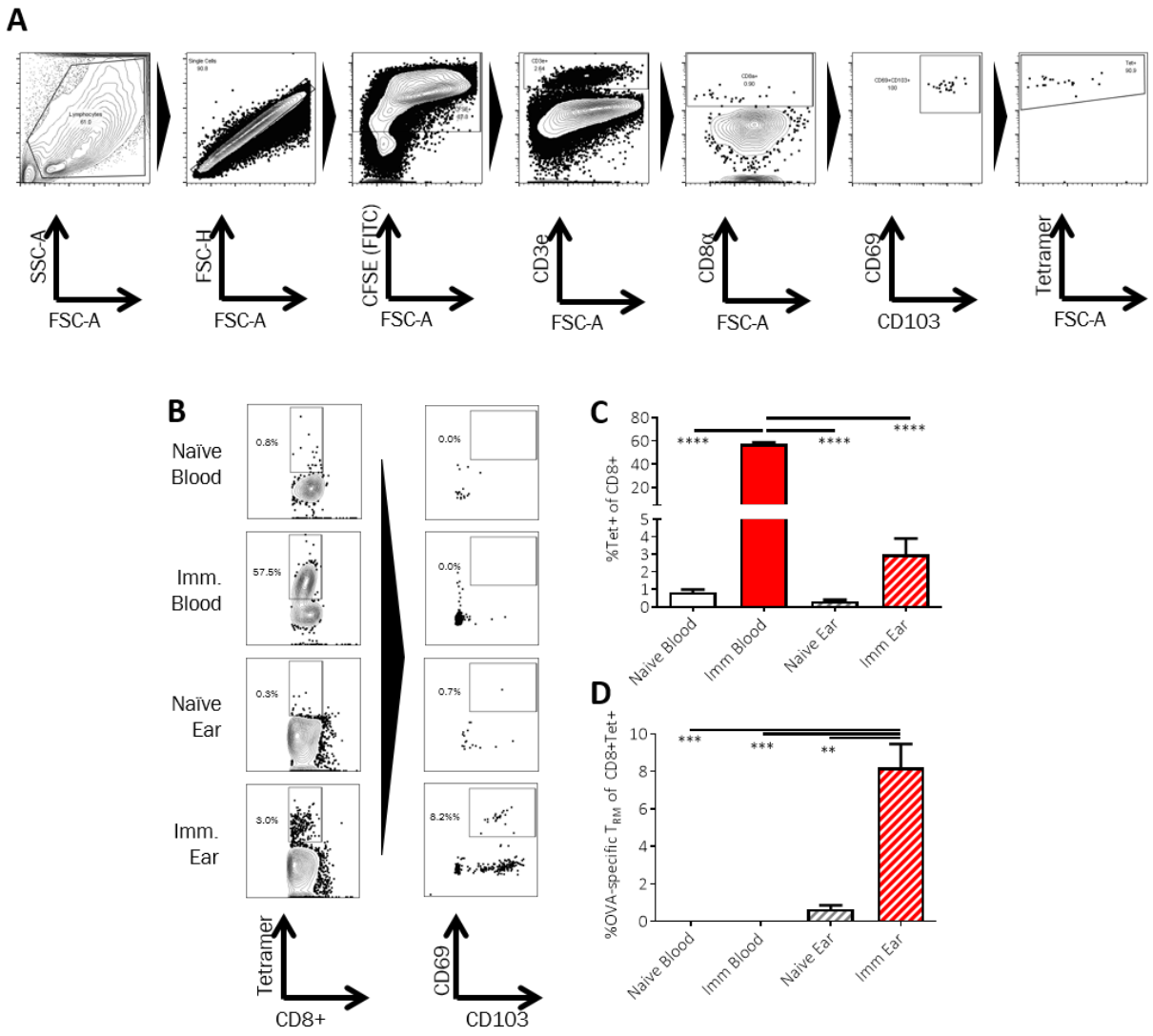

Figure S2: T_{RM} characterization in the blood and skin compartments in OVA-immunized mouse model. Groups of OVA-immunized C57Bl/6 mice (*n*=3/group) were bled, euthanized and their ears were digested and analyzed via flow cytometry. **(A)** Representative flow cytometric plots showing gating strategy for characterizing T_{RM}s in blood and digested ear tissue from mice that are naïve ("Naïve Blood", "Naïve Ear") or were immunized ("Imm. Blood", "Imm. Ear") with OVA. **(B-C)** Representative flow cytometry plots **(B)** and enumeration from groups of mice **(C)** of frequency of OVA tetramer (SIINFEKL/H-2K^b)$^+$ cells among CD8$^+$ cells. **(D)** Frequency of OVA-specific CD8$^+$ cells that are T_{RM} (CD69$^+$CD103$^+$). Data shown are mean ± s.e.m. from one representative experiment of three independent experiments. ****, $p < 0.0001$, analyzed by one-way ANOVA, followed by Tukey's HSD.

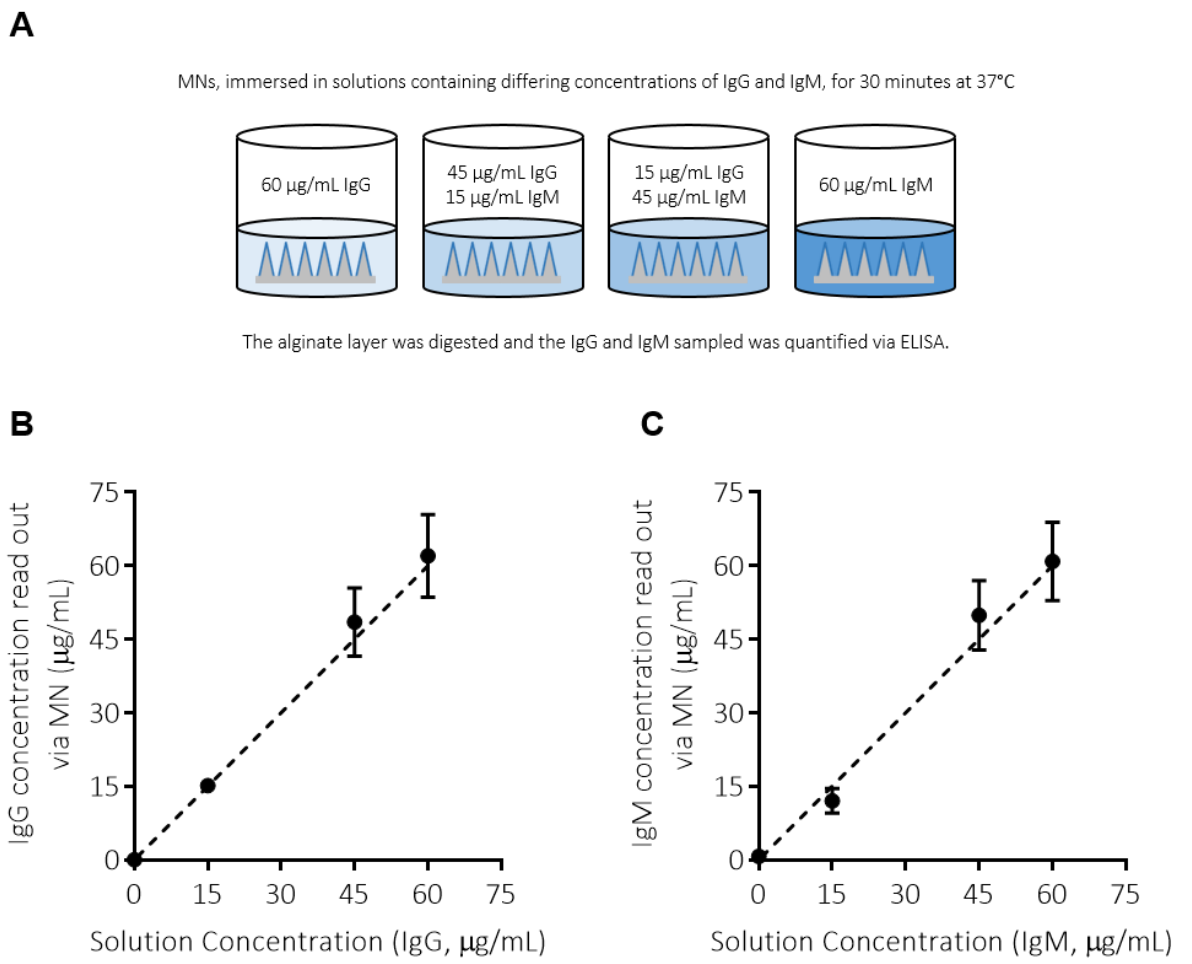

Figure S3. Analysis of fluids recovered from MNs accurately reports on surrounding solution concentrations. (A) Schematic of experiment to test the accuracy of protein quantification via sampling MNs. Briefly, sampling MNs were immersed in solutions containing differing concentrations of IgG and IgM model proteins. The alginate layer was then digested and the resulting solution was quantified via ELISA for IgG **(B)** and IgM **(C)** showing reliable quantification of proteins via sampling MNs.

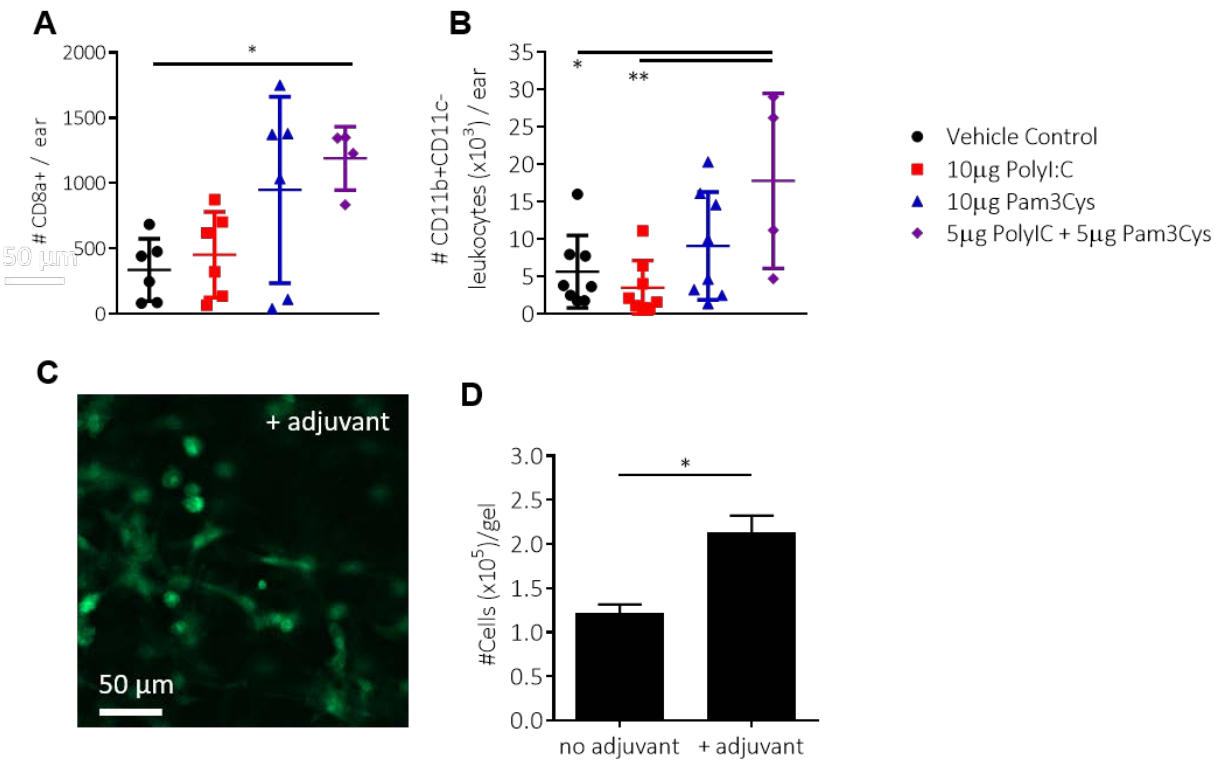

Figure S4: Cell recruitment is enhanced with the inclusion of adjuvants in the alginate hydrogel coating. (A and B) Groups of C57Bl/6 mice (*n*=6/group) were injected intradermally in their ears with adjuvants. Mice were euthanized 48 hours later and ears were digested and analyzed using flow cytometry for infiltrating populations including $CD11b^{+}CD11c^{-}$ myeloid cells **(A)** and $CD8^{+}$ lymphocytes **(B)**. **(C, D)** Hi MW 1% alginate gels carrying 5 µg polyI:C and 5 µg pam3Cys were injected s.c. in the dorsal flank of EGFP-transgenic mice, and 24 hr later, recovered for confocal microscopy and cell counting. **(C)** Confocal microscopy images of GFP^{+} cells infiltrating gels. **(D)** Enumeration of live cells recruited into subcutaneously injected gels under the dorsal flank of naïve C57BL6 mice for 24 hours with and without presence of adjuvants pam3Cys and polyI:C. Data shown are mean ± s.e.m. from one representative experiment of three independent experiments, *, $p < 0.05$ and **, $p < 0.01$, analyzed by one-way ANOVA, followed by Tukey's HSD.

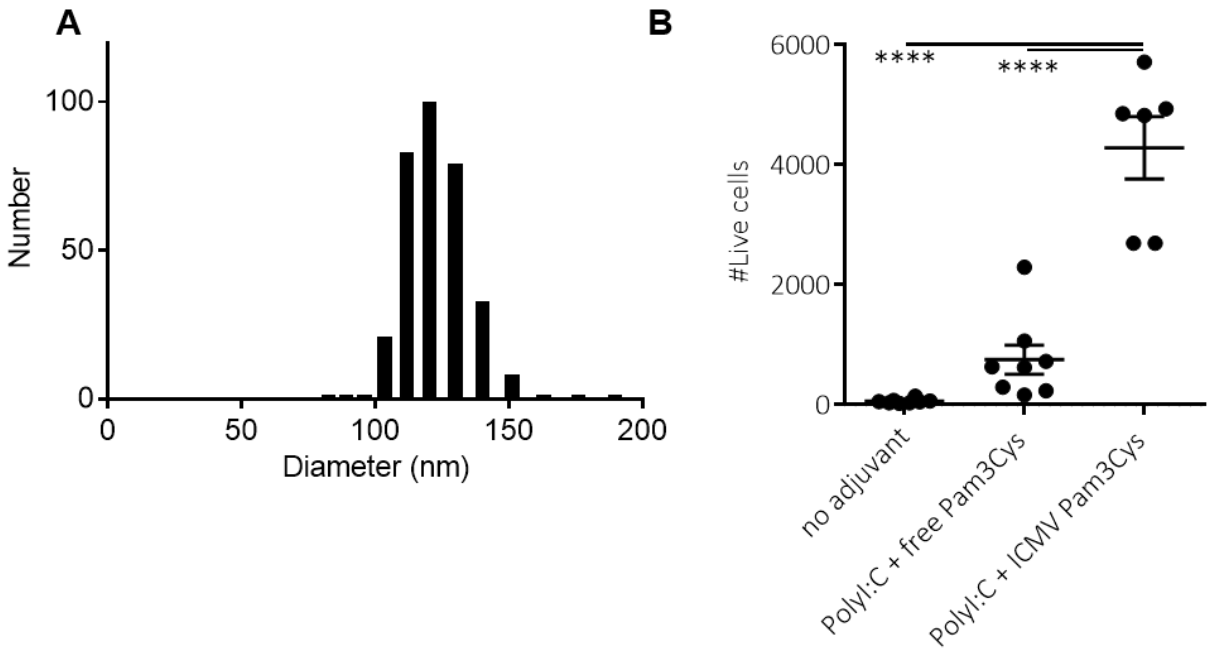

Figure S5: ICMVs encapsulating antigen and adjuvant, when embedded in the alginate layer of sampling MNs, elicit increased recruitment of cells into sampling MNs. (A) Characterization of ovalbumin and pam3Cys-loaded ICMVs via dynamic light scattering. Mean diameter = 126 nm. **(B)** Sampling MNs containing no adjuvant or loaded with 5 µg polyI:C and ICMVs carrying 5 µg pam3Cys in the alginate layer were applied for 12 hr to the ear skin of naïve C57BL/6 mice (*n*=8/group). Shown is enumeration of total live cells retrieved, per MN array. Data shown are mean ± s.e.m. from one representative experiment of two independent experiments, ****, $p < 0.0001$, analyzed by one-way ANOVA, followed by Tukey's HSD.

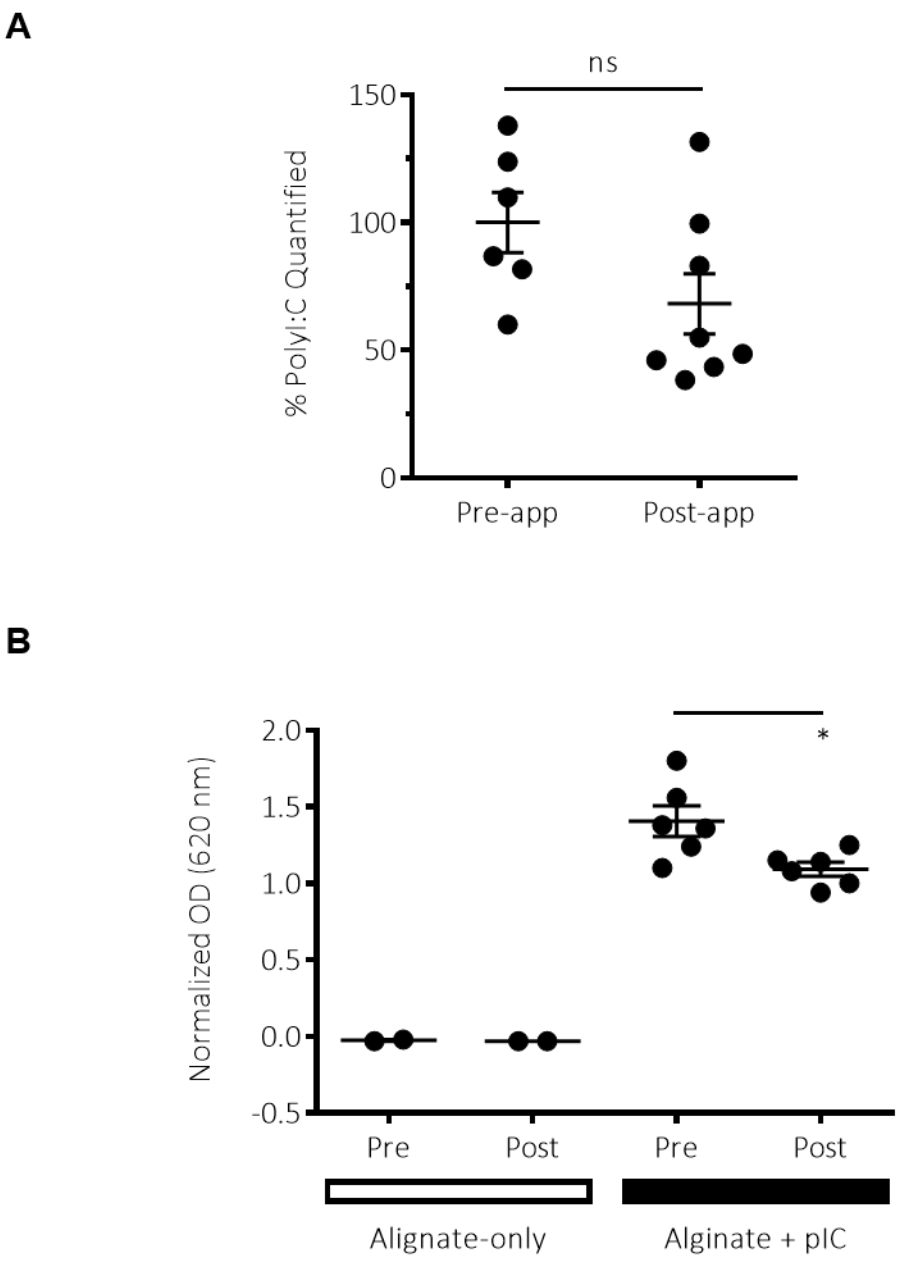

Figure S6: The activity of polyI:C is retained upon incorporation within sampling MNs. (A) MNs loaded with rhodamine-labeled polyI:C were quantified via rhodamine fluorescence pre and post 24 hour application to mouse ears. **(B)** TLR3-expressing HEK blue cells were stimulated with digests from MNs containing alginate only or alginate loaded with polyI:C, and quantified via a colorimetric assay for activation. Data shown are mean ± s.e.m. from one representative of two independent experiments, ns, nonsignificant, *, $p < 0.05$, analyzed by one-way ANOVA, followed by Tukey's HSD.

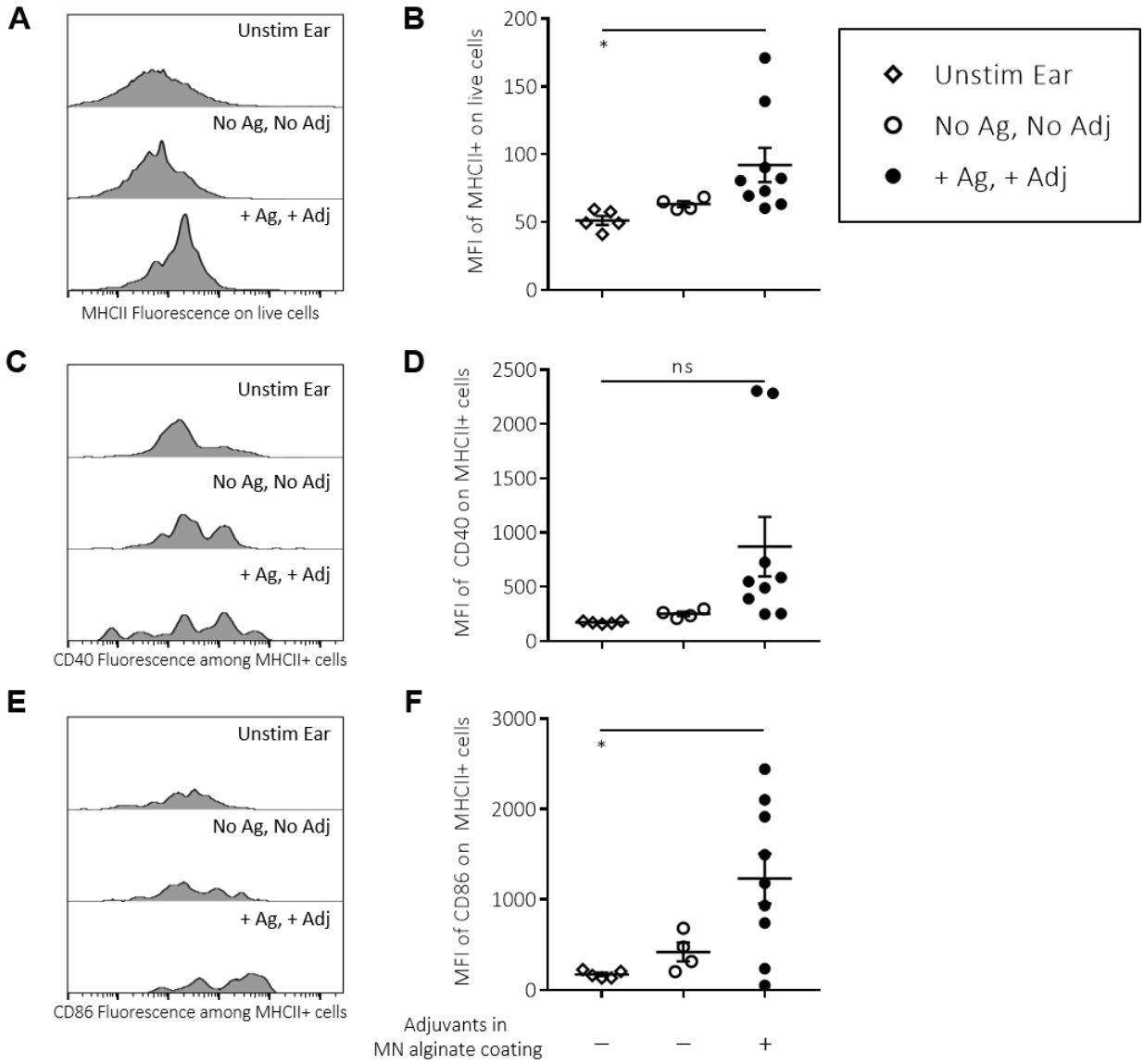

Figure S7: SSMNs containing adjuvants activate recruited APCs. Groups of 10 wk old naïve C57BL/6 mice were either left untreated (open diamonds), or treated for 24 hours with MNs containing either no antigen or adjuvant (open circles) or SSMNs (solid circles). The naïve ear skin and cells sampled via MNs were characterized by flow cytometry. **(A)** Histograms of MHCII fluorescence among live cells, **(B)** median fluorescent intensity (MFI) of MHCII on live cells, **(C)** histograms of CD40 fluorescence on $MHCII^+$ cells, **(D)** MFI of CD40 on $MHCII^+$ cells, **(E)** histograms and CD86 fluorescence on $MHCII^+$ cells, and **(F)** MFI of CD86 on $MHCII^+$ cells. Data shown are mean ± s.e.m. from one representative of two to three independent experiments. ns, nonsignificant, *, $p<0.05$, analyzed by one-way ANOVA, followed by Tukey's HSD.

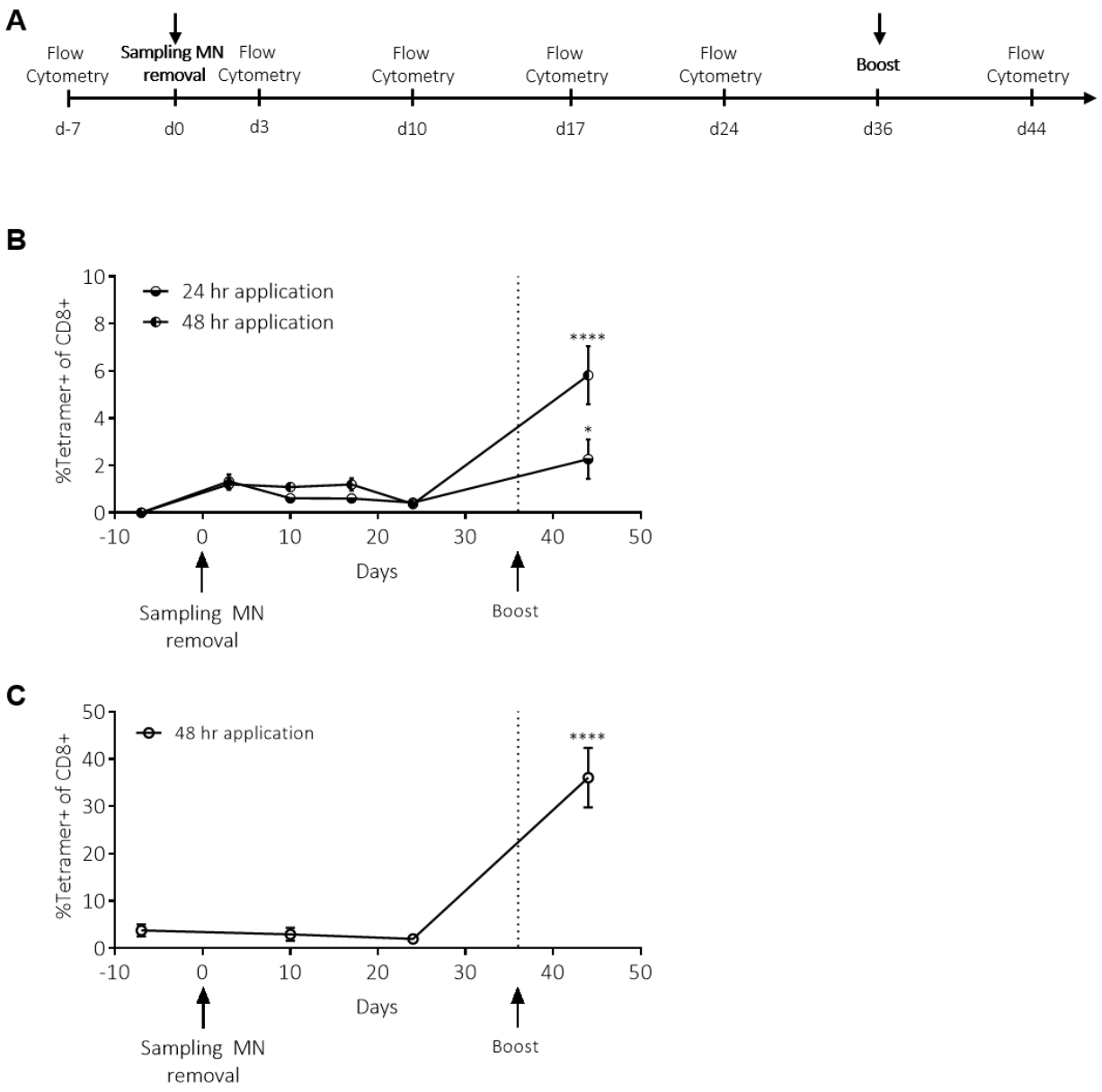

Figure S8: SSMN application for up to 48 hours does not change the immune status of the animal. SSMNs containing adjuvants and ICMVs loaded with 2 μg of OVA were applied to the ear skin of naïve or OVA-immunized C57Bl/6 mice (*n*=5/group) for 24 hours or 48 hours, then retrieved and analyzed via flow cytometry. Shown are experimental timeline **(A),** quantification of OVA-specific $CD8^+$ T cells from blood in naïve **(B)** and previously immunized **(C)** mice, before and after SSMN application at day 0 and vaccination on day 36. Data shown are mean ± s.e.m. from one representative of two independent experiments. ****: $p < 0.0001$ analyzed by one-way ANOVA, followed by Tukey's HSD.

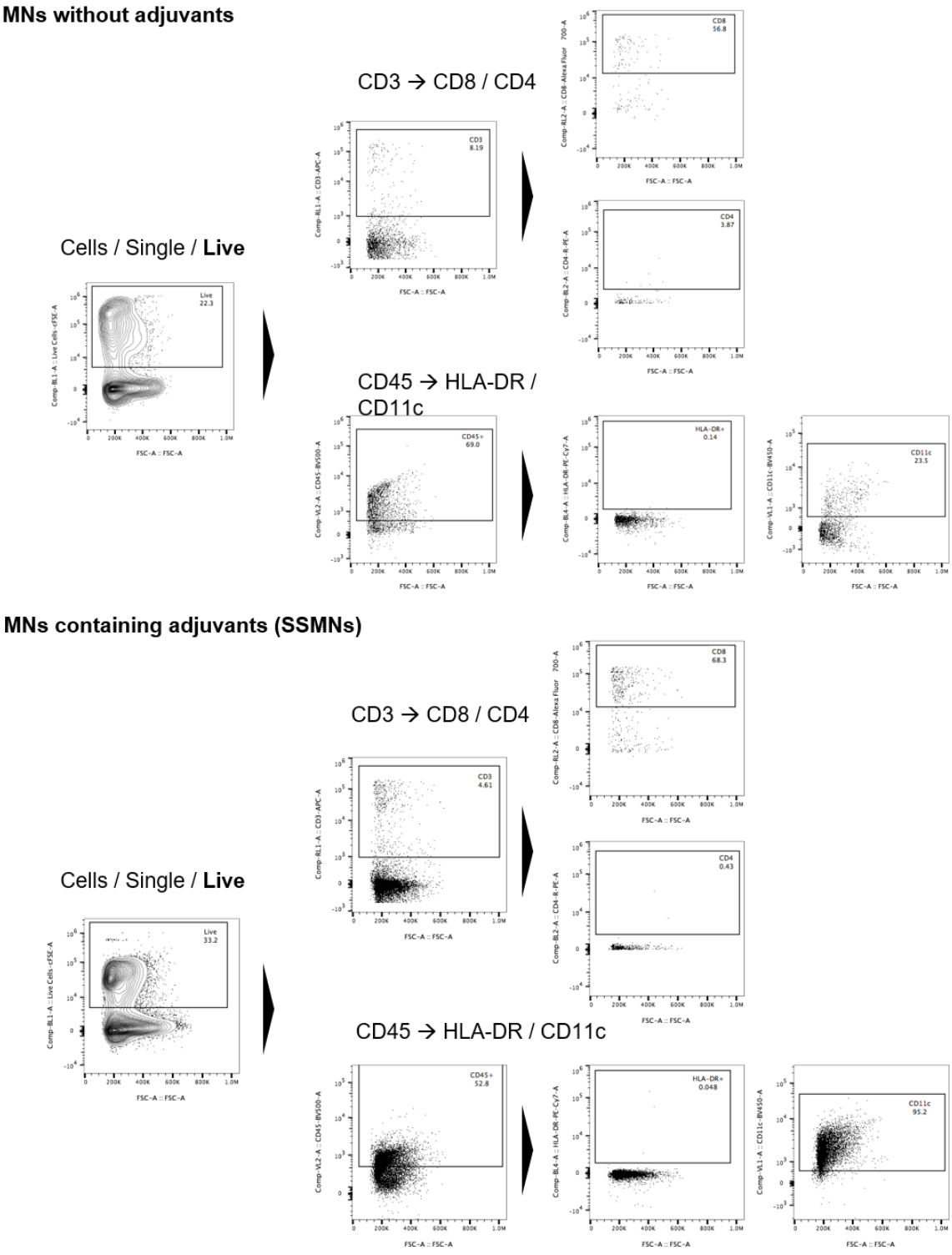

Figure S9: Gating strategy for cells obtained from sampling MNs applied to human skin. Sampling MNs, with and without adjuvants, were applied to excised human skin, and the cells sampled via MNs were analyzed via flow cytometry. Shown here are sample flow cytometric plots showing gating strategy for characterizing $CD8^+$ and $CD11c^+$ cells from human skin via sampling MNs.